

ON EXTENDING THE MASS-METALLICITY RELATION OF GALAXIES BY 2.5 DECADES IN STELLAR MASS

HENRY LEE¹, EVAN D. SKILLMAN¹, JOHN M. CANNON², DALE C. JACKSON¹,
ROBERT D. GEHRZ¹, ELISHA F. POLOMSKI¹, AND CHARLES E. WOODWARD¹

Full version available at <http://www.astro.umn.edu/~hlee/papers/>

ABSTRACT

We report 4.5 μm luminosities for 27 nearby ($D \lesssim 5$ Mpc) dwarf irregular galaxies measured with the *Spitzer* Infrared Array Camera. We have constructed the 4.5 μm luminosity-metallicity ($L-Z$) relation for 25 dwarf galaxies with secure distance and interstellar medium oxygen abundance measurements. The 4.5 μm $L-Z$ relation is $12+\log(\text{O}/\text{H}) = (5.78 \pm 0.21) + (-0.122 \pm 0.012) M_{[4.5]}$, where $M_{[4.5]}$ is the absolute magnitude at 4.5 μm . The dispersion in the near-infrared $L-Z$ relation is smaller than the corresponding dispersion in the optical $L-Z$ relation. The subsequently derived stellar mass-metallicity (M_*-Z) relation is $12+\log(\text{O}/\text{H}) = (5.65 \pm 0.23) + (0.298 \pm 0.030) \log M_*$, and extends the SDSS M_*-Z relation to lower mass by about 2.5 dex. We find that the dispersion in the M_*-Z relation is similar over five orders of magnitude in stellar mass, and that the relationship between stellar mass and interstellar medium metallicity is similarly tight from high-mass to low-mass systems. We find a larger scatter at low mass in the relation between effective yield and total baryonic mass. In fact, there are a few dwarf galaxies with large yields, which is difficult to explain if galactic winds are ubiquitous in dwarf galaxies. The low scatter in the $L-Z$ and M_*-Z relationships are difficult to understand if galactic superwinds or blowout are responsible for the low metallicities at low mass or luminosity. Naively, one would expect an ever increasing scatter at lower masses, which is not observed.

Subject headings: galaxies: dwarf — galaxies: evolution — galaxies: irregular — infrared: galaxies

1. INTRODUCTION

The luminosity-metallicity ($L-Z$) relation for gas-rich star-forming galaxies is a robust relationship which holds over ten magnitudes in galaxy optical luminosity (e.g., Zaritsky et al. 1994; Tremonti et al. 2004). The physical basis for this relation has generally been attributed to a mass-metallicity relation for galaxies. The $L-Z$ relation has also become an important tool to examine the time-evolution of past chemical enrichment and the (stellar) mass-metallicity (M_*-Z) relation for more massive galaxies at distant epochs, where emission lines at rest-frame optical wavelengths are redshifted into the near-infrared; see, e.g., Kobulnicky & Zaritsky (1999); Kobulnicky et al. (2003); Liang et al. (2004); Kobulnicky & Kewley (2004); Shapley et al. (2004); Gallazzi et al. (2005); Hoyos et al. (2005); Maier et al. (2005); Savaglio et al. (2005); Shapley et al. (2005); Erb et al. (2006); Lamareille et al. (2006); Liang et al. (2006). The growing body of observations at intermediate- and high-redshifts has led to work on a variety of galaxy formation models and their subsequent predictions for $L-Z$ and M_*-Z relations (e.g., Somerville & Primack 1999; Bell & Bower 2000; Tamura et al. 2001; Dekel & Woo 2003; De Lucia et al. 2004; Savaglio et al. 2005; Tissera et al. 2005).

For nearby dwarf irregular and other star-forming dwarf galaxies, the corresponding $L-Z$ relation has traditionally been studied at optical wavelengths (e.g., Lequeux et al. 1979; Skillman et al. 1989; Richer & McCall 1995; Skillman et al. 1997; Pilyugin 2001; Garnett 2002; Hidalgo-Gómez et al. 2003; H. Lee et al. 2003a,b,c; Pilyugin et al. 2004; van Zee & Haynes 2006; van Zee et al. 2006). If systematic uncertainties are minimized, the resulting residuals

in the $L-Z$ relation can be used to examine effects of galaxy evolution (e.g., Kobulnicky et al. 2003). However, dispersion in the optical $L-Z$ relation is thought to arise from variations in the stellar mass-to-light ratios, which are caused by variations in the current star formation rate (SFR) among galaxies (see, e.g., Bell & de Jong 2001; Tumlinson 2006). To minimize the effects of these variations, the $L-Z$ relation can be determined at near-infrared (NIR; 1–5 μm) wavelengths, where the dominant emission arises from the stellar populations.

Recent ground-based efforts to determine $L-Z$ and M_*-Z relations for low-mass systems in the NIR have been constructed and described by, e.g., Pérez-González et al. (2003), J. Lee et al. (2004), Salzer et al. (2005), Saviane et al. (2005), Oliveira et al. (2006), and Rosenberg et al. (2006). The sensitivity of the *Spitzer Space Telescope* provides an excellent opportunity to observe total emission from the stellar populations in nearby dwarf galaxies, because most of these systems are of intrinsically low surface brightness, and are therefore highly challenging to observe in the NIR from the ground (e.g., Vaduvescu et al. 2005). The 4.5 μm luminosities are dominated by emission from stellar photospheres (e.g., Lu et al. 2003; Dale et al. 2005; Galliano 2005), and are less sensitive to bursts of star formation. Observations at 4.5 μm were chosen also because the passband was designed to avoid emission from polycyclic aromatic hydrocarbons (PAHs; e.g., Léger & Puget 1984; Allamandola et al. 1985). PAH emission does not appear to be significant within lower-luminosity metal-poor galaxies (e.g., Houck et al. 2004; Engelbracht et al. 2005; Hogg et al. 2005). Although emission from hot dust might be significant in disk galaxies at 4.5 μm (e.g., Roussel et al. 2005), our 8 μm observations have shown that the contributions from PAHs and warm dust are not significant in our sample of low-mass dwarf galaxies (Jackson et al. 2006).

In light of the M_*-Z relation for massive galaxies determined by Tremonti et al. (2004), we consider nearby dwarf

¹ Department of Astronomy, University of Minnesota, 116 Church St. S.E., Minneapolis, MN 55455; hlee, skillman, djackson, gehrz, elwood, chelsea@astro.umn.edu

² Max-Planck-Institut für Astronomie, Königstuhl 17, D-69117 Heidelberg, Germany; cannon@mpia.de

galaxies, which extend the mass range down by roughly 2.5 dex. This allows us to examine the M_* - Z relation over five orders of magnitude in stellar mass. To construct the L - Z and M_* - Z relations at $4.5 \mu\text{m}$, we have chosen nearby star-forming dwarf irregular galaxies that have distances measured from stellar constituents, and oxygen abundances derived from high-quality spectra (namely, [O III] $\lambda 4363$ measurements). We have assembled a sample of 27 dwarf galaxies at distances below about 5 Mpc; some properties of these dwarf galaxies are listed in Table 1.

The remainder of this paper proceeds as follows. Those who wish to skip the details should go directly to § 7, where we interpret our key results in the context of the findings by Tremonti et al. (2004). Observations and reductions of the data are presented in § 2. We describe the measurements of flux densities and absolute magnitudes of dwarf galaxies at $4.5 \mu\text{m}$, and the corresponding NIR L - Z and M_* - Z relations in §§ 3 and 4. We have also gathered from the literature other L - Z and M_* - Z relations for local and distant star-forming galaxies. As all of the galaxies in our sample have direct measurements of their H I gas, we also examine relations with gas-to-stellar mass ratio and H I rotation velocity in §§ 5 and 6, respectively. We give additional discussion and a summary in §§ 7 and 8, respectively. For the present discussion, we use the notation $[\text{O}/\text{H}] = \log(\text{O}/\text{H}) - \log(\text{O}/\text{H})_{\odot}$, where the solar value of the oxygen abundance is $12 + \log(\text{O}/\text{H}) = 8.66$ (Asplund et al. 2004; Meléndez 2004). We adopt $Z_{\odot} = 0.0126$ as the revised solar mass fraction in the form of metals (Asplund et al. 2004).

2. OBSERVATIONS AND REDUCTIONS

Data were acquired with the Infrared Array Camera (IRAC; Fazio et al. 2004) on the *Spitzer Space Telescope* (Werner et al. 2004) during the first year of nominal operations from 2003 December to 2004 December. In Guaranteed Time Observation (GTO) program 128 (P.I. R.D. Gehrz), ten galaxies were imaged in channels 2 ($4.5 \mu\text{m}$) and 4 ($8 \mu\text{m}$). The Astronomical Observation Request Key (AORKEY) for each galaxy is listed in Table 1. We performed five dither positions per pointing with exposure times of 200 seconds each, except for NGC 55 and WLM which had exposure times of 100 seconds per dither position. A single $5' \times 5'$ pointing was used for all targets, except for IC 1613, NGC 55, NGC 3109, and WLM, which were mosaicked in array coordinates using a 2×2 ($10' \times 10'$), a 1×2 ($5' \times 10'$), and a 1×3 ($5' \times 15'$) pointing grid, respectively. NGC 55 was mosaicked in sky coordinates, resulting in a $15' \times 10'$ field-of-view. Using the MOPEX³ reduction package, the final mosaics were created as described in Jackson et al. (2006). These images contained the appropriate astrometry in Epoch J2000 coordinates and were flux-calibrated in units of MJy sr^{-1} . Postage-stamp images at $4.5 \mu\text{m}$ of ten galaxies from program GTO 128 are shown in Fig. 1; note that the galaxies are displayed with the same isophotal scaling to emphasize the large range in surface brightness.

Total photometry was obtained with the application of elliptical apertures, and adjusting the dynamic range to show the spatial extent of the emission at $4.5 \mu\text{m}$. We also retrieved optical images from NED and the Local Group Survey⁴ (Massey et al. 2002), and we “stretched” these images

visually (in intensity scale) in order to discern the outer limit of the optical extent and to compare the spatial extents of the optical and NIR luminosities. Elliptical apertures were constructed to optimize the amount of light measured for each target galaxy. Six to seven circular apertures in the immediate vicinity of the elliptical aperture were used to sample and determine the mean background level surrounding the galaxy. This method benefits from the sampling of both the sky and the foreground stellar contamination. An example is shown in Fig. 2. We used the IRAF⁵ task *polyphot* to perform the aperture photometry and measure flux densities. A variety of tests were performed to mask and remove negative pixels, bright foreground stars, and bright pixels caused by “bleeding” from bright stars. Additional experiments (varying the size of the elliptical aperture; increasing the number of circular “background” apertures) were used to test our final photometry results. The subsequent range in derived luminosities falls well within the quoted uncertainties for the distance modulus and the total errors for IRAC flux measurements (see below).

We have also added from the *Spitzer* public data archive eleven dwarf galaxies from the SINGS Legacy program (Kennicutt et al. 2003b), one dwarf galaxy from program GTO 59 (P.I. G. Rieke), and five dwarf galaxies from program GTO 69 (P.I. G. Fazio). To ensure homogeneity in the derived absolute magnitudes at $4.5 \mu\text{m}$, we have performed the same procedure described above to determine total fluxes and luminosities. As shown in Fig. 3, our measured flux densities for the selected SINGS galaxies are consistent with those reported by Dale et al. (2005).

We adopt 10% as the error in the total flux, assuming this is the maximum error of the absolute calibration in channel 2 (Hora et al. 2004). Various image-based corrections (array location dependent photometric correction, pixel-phase correction) in channel 2 are well below the uncertainty in the absolute calibration (Reach et al. 2005), and are not included in this paper. We have applied a correction to account for extended surface brightness by multiplying measured channel 2 fluxes by a factor of 0.937 (Reach et al. 2005) to obtain the appropriate scaled results. With our measured flux densities at $4.5 \mu\text{m}$, we derived absolute magnitudes, $M_{[4.5]}$, by using the adopted zero-magnitude flux density, $F_{[4.5]}^0 = 179.7 \pm 2.6$ Jy (Reach et al. 2005). We have also assumed zero extinction at $4.5 \mu\text{m}$ (e.g., Lutz 1999; Indebetouw et al. 2005), and negligible contribution by diffuse H I Brackett- α emission to the overall galaxy flux (e.g., Lu et al. 2003; Lu 2004).

A comparison between B and $4.5 \mu\text{m}$ luminosities is shown in Fig. 4, where B luminosities corrected for Galactic extinction are taken from Karachentsev et al. (2004). For the remainder of this paper, we will refer to IRAC channel 2 luminosities as “[4.5]”. Galaxy luminosities at $4.5 \mu\text{m}$ are also plotted against B -[4.5] color; no correlation is evident. The mean B -[4.5] color for our sample in Table 1 is 2.08 ± 0.59 , which is consistent with the range of observed B - K colors for a sample of nearby late-type dwarf galaxies in 2MASS (Jarrett et al. 2003).

3. THE NEAR-INFRARED LUMINOSITY-METALLICITY RELATION

<http://www.lowell.edu/users/massey/lgsurvey.html>.

⁵ IRAF is distributed by the National Optical Astronomical Observatories, which are operated by the Associated Universities for Research in Astronomy, Inc., under cooperative agreement with the National Science Foundation.

³ MOPEX is available from the *Spitzer* Science Center at <http://ssc.spitzer.caltech.edu/postbcd/>.

⁴ More about the Local Group Survey is found at

Twenty-five dwarf galaxies in our sample have reported oxygen abundances, and 21 dwarf galaxies have oxygen abundances derived from [O III] $\lambda 4363$ measurements (Table 1). In the absence of [O III] $\lambda 4363$, oxygen abundances for DDO 53, Ho I, and NGC 3109 were derived using the McGaugh (1991) bright-line calibration⁶. We adopt for Peg DIG the oxygen abundance derived by Skillman et al. (1997). We have assumed oxygen abundances are spatially homogeneous in dwarf irregular galaxies (e.g., Kobulnicky & Skillman 1997; Kobulnicky et al. 1997; H. Lee & Skillman 2004; H. Lee et al. 2005, 2006a).

To obtain fits between absolute magnitude and oxygen abundances for our sample of dwarf galaxies in B and at $4.5 \mu\text{m}$, we used the ordinary least squares bisector method (see Akritas & Bershady 1996, and references therein). Specifically, these are bivariate least-squares fits with the bisector method incorporating heteroscedastic errors (in both luminosity and oxygen abundance). The two fits are expressed as

$$\begin{aligned} 12 + \log(\text{O}/\text{H}) &= (5.94 \pm 0.27) + (-0.128 \pm 0.017)M_B \quad (1) \\ &= (5.78 \pm 0.21) + (-0.122 \pm 0.012)M_{[4.5]}, \quad (2) \end{aligned}$$

where M_B is the absolute magnitude in B , corrected for Galactic extinction (Karachentsev et al. 2004), and $M_{[4.5]}$ is the absolute magnitude at $4.5 \mu\text{m}$, respectively. The fits in B and $[4.5]$ are shown in Fig. 5. The slopes, intercepts, and their corresponding errors are computed with the bi-variate correlated errors and scatter regression code⁷, where we have assumed uncorrelated errors and set the covariance to zero. The resulting errors incorporate uncertainties associated with the data points being fitted. All of the fits below use the same technique, and we refer to this procedure as the “bisector” method⁸. The fit at B is consistent with similar fits obtained by, e.g., H. Lee et al. (2003b), van Zee & Haynes (2006), and van Zee et al. (2006). The NIR slope is marginally smaller than the optical slope, although the derived slopes and intercepts for both $L-Z$ relations are consistent with each other.

Variations in the stellar mass-to-light ratio can be responsible for some or all of the scatter in the $L-Z$ relation. Moreover, the optical luminosity of a fainter galaxy is affected more by a burst of new star formation than the luminosity of a brighter galaxy. Skillman et al. (1997) proposed a comparison of the residuals in luminosity against color to test whether variations in the stellar mass-to-light ratio were the main cause of the scatter. A limited set of data at the time were plotted against optical $B-V$ color, and were suggestive of a correlation between the residuals in B luminosity versus $B-V$.

We show now that the scatter in the $L-Z$ relation diminishes when luminosities are measured at longer wavelengths. Residuals in oxygen abundance are plotted against B and $[4.5]$ absolute magnitude in the top and bottom panels, respectively, of Fig. 6. The dispersions in the optical and NIR $L-Z$ relations are 0.161 dex and 0.122 dex, respectively. The scatter in the NIR $L-Z$ relation is reduced compared to the optical $L-Z$ relation. The dispersion in the $L-Z$ relation was *expected* to decrease at longer wavelengths, as NIR luminosities are less

sensitive to extinction by dust and variations in the present-day SFR.

The smaller slope and the reduced dispersion in the NIR are in agreement with the results for star-forming galaxies in the field reported by Salzer et al. (2005). Higher-luminosity and higher-mass galaxies contain more metals and more dust (e.g., Rosenberg et al. 2006); these galaxies would be optically underluminous, which would yield a steeper slope in the optical $L-Z$. The effects of absorption by dust vary from galaxy to galaxy, which introduces greater overall scatter in the optical $L-Z$. Absorption by dust is mitigated in the NIR, which produces an $L-Z$ relation with a shallower slope and less scatter. For our present sample of dwarf galaxies, we have assumed that dust is less important (see § 1) than the variations in stellar mass-to-light ratios.

We now examine residuals in oxygen abundance and luminosity against $B-[4.5]$ color. The results are shown in Fig. 7. Residuals in oxygen abundance from the $B L-Z$ relation are correlated with color in the sense that redder galaxies have larger abundances compared to the best fit. On the other hand, there is very little to no trend with color for the residuals from the $[4.5] L-Z$ relation. Residuals in magnitude from the optical and infrared $L-Z$ relations exhibit similar behavior as above; redder galaxies are fainter in B and no trend is found at $4.5 \mu\text{m}$. The plots in Fig. 7 clearly show that the dispersion is clearly reduced at NIR wavelengths.

We compare in Table 2 the $4.5 \mu\text{m} L-Z$ relation with recent optical and NIR $L-Z$ relations from the literature. The slopes from our optical and NIR relations are smaller than values derived from similar relations for other samples of nearby dwarf galaxies. In addition to listing the slope and intercept values for each $L-Z$ relation, we have also computed the oxygen abundance from the specified relation at a fiducial galaxy luminosity equal to $M_\lambda = -16$. The key result from the comparison is that our NIR $L-Z$ relation exhibits the smallest dispersion.

4. STELLAR MASS-METALLICITY RELATION

The NIR $L-Z$ relation reflects a fundamental relation between underlying stellar mass and metallicity, and thus, NIR luminosities of dwarf galaxies can directly be related to the mass of their stellar populations (e.g., Vaduvescu et al. 2005). First, to derive the $4.5 \mu\text{m}$ luminosity in solar units, we have assumed that the absolute magnitude of the Sun is $+3.33$ in K (Bell & de Jong 2001), and that the ground-based $K-M$ color⁹ is about 0 for a G2 dwarf star (e.g., Bessell & Brett 1988). Thus, we assume that the absolute magnitude of the Sun at $4.5 \mu\text{m}$ is $\simeq +3.3$. Even if the NIR luminosity is dominated by giant stars, the most extreme $K-[4.5]$ colors are between $+0.1$ and -0.1 . As we show below, a non-zero $K-[4.5]$ color introduces a zero-point offset in the M_*-Z relation.

We consider an appropriate stellar mass-to-NIR-light ratio. We first assumed a constant stellar mass-to- $[4.5]$ -light ratio of 0.5, as motivated by models for the formation of disk galaxies (e.g., van den Bosch 2002). This value of the stellar mass-to-light ratio is assumed to be independent of color. The resulting fit to the stellar mass-metallicity relation is $12 + \log(\text{O}/\text{H}) = (5.26 \pm 0.27) + (0.332 \pm 0.033) \log M_*$, and the resulting dispersion is 0.125 dex. However, stellar mass-to-light ratios can vary by a factor of ~ 2 , even at NIR wavelengths (e.g., Bell & de Jong 2001). Fortunately, stellar mass-to-NIR light

⁶ Analytical expressions for the calibration are found in Kobulnicky et al. (1999). Measurements of [N II]/[O II] ($\lesssim 0.1$) break the double-valued degeneracy and point to the “lower branch,” which is appropriate for dwarf galaxies; see H. Lee & Skillman (2004) for additional discussion.

⁷ The code is available from STATCODES: <http://www.astrostatistics.psu.edu/statcodes/>.

⁸ For each fit, we perform 10000 “bootstrap” simulations to converge onto a solution with the appropriate errors.

⁹ We assume that the effective wavelength of M is $4.8 \mu\text{m}$ (Campins et al. 1985).

ratios are not strongly dependent upon the age of the dominant stellar population.

For the next step, we derived stellar mass-to-light ratios by accounting for color variations. We used the models by Bell & de Jong (2001, their Tables 3 & 4), where the authors developed methods to derive better estimates of stellar mass in disk galaxies and to determine the baryonic Tully-Fisher relation. For each model in Bell & de Jong (2001), we derived a mass-to-light ratio as a linear function of $B-K$ color, and computed the stellar mass for each galaxy. Using the color-based functions for $B-V$ and $V-K$, we applied a simple linear combination to obtain the stellar mass-to-light ratio as a linear function of $B-K$ color. We write

$$\log(M_*/L_K) = a' + b'(B-K), \quad (3)$$

where a' and b' are given in Table 3, and $B-K = (B-[4.5]) - (K-[4.5])$ using our measured $B-[4.5]$ colors. For a small sample of late-type galaxies, Pahre et al. (2004) determined $K-[4.5]$ in the range between -0.1 and $+0.4$. We adopt here $K-[4.5] = +0.2$, and subsequent stellar masses are 0.15 to 0.16 dex smaller than stellar masses derived with $K-[4.5] = 0$.

We obtain stellar masses with

$$\begin{aligned} \log M_* &= \log(M_*/L_K) + \log L_K \\ &= \log(M_*/L_K) + [\log L_{[4.5]} - 0.4(K-[4.5])], \end{aligned} \quad (4)$$

with the stellar mass-to-light ratio defined above. With this empirical prescription for stellar masses, we subsequently performed a M_*-Z fit to each model. The results are shown in Table 3. Although stellar masses for a given galaxy can vary by as much as ~ 0.5 dex from model-to-model, the subsequent M_*-Z fits spanning a range of about four decades in stellar mass are similar for all models. The M_*-Z slopes for models at subsolar metallicity are marginally smaller than the scaled Salpeter stellar initial mass function (IMF) models at solar metallicity.

For this work, we used model 8 in Table 3 (Salpeter IMF, subsolar metallicity) and Equations (3) and (4) to derive initial stellar masses. We then subtracted 0.25 dex from all of the stellar masses to scale the masses from the Salpeter (1955) IMF to the Chabrier (2003) IMF. Tremonti et al. (2004) used the Kroupa (2001) IMF to derive stellar masses, which are about 0.30 dex smaller than masses derived with the Salpeter IMF; Bell et al. (2003) provide additional discussion on using different IMFs to derive stellar masses in late-type galaxies. We adopt the errors in $[4.5]$ absolute magnitude as the errors in the logarithm of the stellar mass. We note that our derived stellar mass for NGC 6822, $\log(M_*/M_\odot) = 8.10$, is consistent with the value (8.24) derived from an independent model describing the photometric and chemical evolution (Carigi et al. 2006).

The final M_*-Z relation is expressed as

$$12 + \log(\text{O}/\text{H}) = (5.65 \pm 0.23) + (0.298 \pm 0.030) \log M_*. \quad (5)$$

The dispersion is 0.117 dex. In Fig. 8, we show the data and the fit expressed by Equation (5) in panel (a). We find an excellent correlation between oxygen abundance and stellar mass; the Pearson correlation coefficient is $r = +0.90$. No trend is seen in a plot of the residuals in oxygen abundance from the M_*-Z relation against stellar mass in panel (b).

We compare our M_*-Z relation with the relation recently derived for massive galaxies. Tremonti et al. (2004) derived the M_*-Z relation for over 53000 massive star-forming galaxies at redshifts $z \lesssim 0.1$ from the Sloan Digital Sky Survey

(SDSS). In Fig. 9, we show the full range in both axes, spanning over two orders of magnitude in oxygen abundance, and five orders of magnitude in stellar mass. The data presented here extend the SDSS M_*-Z relation to lower masses by roughly 2.5 dex. The dispersion for our M_*-Z relation is comparable to that of the SDSS M_*-Z relation (≈ 0.1 dex). If dwarf galaxies have insufficient total masses to retain ejecta from supernovae, we expect that the dispersions in both $L-Z$ and M_*-Z relations should increase with decreasing luminosity and mass. We will discuss the implications of our $L-Z$ and M_*-Z results in § 7.

The polynomial fit to the SDSS galaxies is effective in the mass range between $10^{8.5}$ and $10^{11.5} M_\odot$, whereas our relation overlaps the SDSS relation in the mass range between $10^{8.5}$ and $10^{9.5} M_\odot$. At these stellar masses, SDSS galaxies are about 0.2–0.3 dex more metal-rich than the present sample of dwarf galaxies. We describe here the most likely reasons for the offset; see also Savaglio et al. (2005). First, SDSS fiber spectra preferentially sample the inner $\approx 25\%$ of galaxies (Tremonti et al. 2004). Given that nearby spirals exhibit radial metallicity gradients (e.g., Zaritsky et al. 1994), derived abundances from SDSS spectra might be too high for a number of the galaxies. Second, oxygen abundances for the SDSS data were derived using bright-line methods in the absence of the temperature-sensitive [O III] $\lambda 4363$ emission line. Recent work with nearby spiral galaxies has shown that bright-line oxygen abundances overestimate the true oxygen abundances by roughly 0.2 to 0.3 dex at metallicities solar and above (e.g., Stasińska 2002; Kennicutt et al. 2003a; Bresolin et al. 2004). These effects together can account for the offset between the present sample of dwarf galaxies and the SDSS sample of higher-mass galaxies.

Fig. 9 suggests two intriguing possibilities: (a) over a large range in mass ($\simeq 5.5$ dex) there is a single and continuous M_*-Z relation which turns over or flattens at high galaxy mass, or (b) the M_*-Z relations describing dwarf and giant galaxies may have different slopes; this possibility has also been suggested by e.g., Salzer et al. (2005); Rosenberg et al. (2006). It will be very interesting to investigate whether slopes of the $L-Z$ and M_*-Z relations exhibit a “break” at some characteristic luminosity and mass, respectively¹⁰.

In Table 4, we list the M_*-Z relation from the present work, as well as other relations from the literature. With increasing numbers of intermediate- and high-redshift galaxies with measured luminosities and abundances, the interpretation of the M_*-Z relation for massive systems at distant epochs will depend upon the specific bright-line calibration used to derive oxygen abundances. Although selection criteria and the methods used to derive masses and metallicities may vary, comparisons which begin to tie relations between high-mass and low-mass galaxies and between local and distant galaxies may help illustrate processes acting on galaxies over a range in mass and redshift.

5. RELATIONS WITH GAS-TO-STELLAR MASS RATIO

We consider the gas-to-stellar mass ratio, which is representative of the baryonic gas fraction (e.g., Garnett 2002;

¹⁰ Examination of the latest SDSS data (~ 80000 objects in DR4; C. Tremonti, personal communication) shows that the subsequent M_*-Z fit is effective to another 0.5 dex lower in mass to $\log(M_*/M_\odot) \sim 8$. Despite the different methods by which stellar masses and oxygen abundances have been determined, there appears to be good agreement at $\log(M_*/M_\odot) \sim 8$ between the upper-end of our M_*-Z relation and the lower-end of the SDSS M_*-Z relation.

H. Lee et al. 2003b; Skillman et al. 2003; van Zee & Haynes 2006). These parameters reveal important information about the conversion of gas into stars and metals, and about possible gas flows. Assuming zero gas flows and instantaneous recycling, the closed-box model of chemical evolution predicts the metallicity by mass Z (Schmidt 1963; Searle & Sargent 1972)

$$Z = y \ln \mu^{-1}, \quad (6)$$

where y is the yield and $\mu = M_{\text{gas}}/(M_{\text{gas}} + M_*)$ is the fraction of total baryonic mass in the form of gas. From the equation above, we can derive the oxygen abundance by number

$$12 + \log(\text{O}/\text{H}) = 12 + \log(y_{\text{O}}/\zeta) + \log(\ln[1 + (M_{\text{gas}}/M_*)^{-1}]), \quad (7)$$

where y_{O} is the oxygen yield by mass, $\zeta = 11.728$ is the factor to convert abundance by mass to abundance by number, $M_{\text{gas}} = 1.36 M_{\text{HI}}$ is the total gas mass (which includes helium), and M_{gas}/M_* is the gas-to-stellar mass ratio, which is independent of distance.

All of the galaxies in the present sample have direct measures of their H I gas content. We have adopted 21-cm flux integrals from the catalog by Karachentsev et al. (2004). However, we have not scaled the H I mass to the spatial extent of the optical or NIR luminosity (re. stellar mass)¹¹. The 21-cm flux integrals and the derived gas-to-stellar mass fractions are listed in Table 5.

The results are shown in Fig. 10. In panel (a), we have plotted oxygen abundances against the gas-to-stellar mass ratio, and the subsequent least-squares fit with the bisector method. The fit is shown as a solid line, and is expressed as

$$12 + \log(\text{O}/\text{H}) = (8.21 \pm 0.07) + (-0.435 \pm 0.085) \log(M_{\text{gas}}/M_*). \quad (8)$$

The dispersion is 0.24 dex. In the center panel (b), we have plotted outflow models as variations of the closed-box model; we assume negligible inflow of metal-poor gas. The purple and blue set of curves, respectively, describe $y_{\text{O}} = 0.01$ (Tremonti et al. 2004) and $y_{\text{O}} = 2 \times 10^{-3}$ (H. Lee et al. 2003b; van Zee & Haynes 2006). For each set of curves, the outflow rates from right to left are 0, 5, 10, 25, and 50 times the star-formation rate. These results suggest reduced yields and/or significant outflow rates, which previous authors (e.g., Garnett 2002; van Zee & Haynes 2006) have also indicated.

In Fig. 10c, we have plotted the $B-[4.5]$ color against the gas-to-stellar mass ratio, where there is a very clear correlation. We first point out three outliers in the data. At $B-[4.5] \approx +1$ and $\log(M_{\text{gas}}/M_*) \approx -0.4$, NGC 1569 is unusually blue for its gas-to-stellar mass ratio, as this dwarf galaxy is known to have just undergone a very strong burst of star formation (e.g., Israel 1988; Waller 1991). At the other end of the plot ($B-[4.5] \approx +2$, $\log(M_{\text{gas}}/M_*) \approx +1.5$) are DDO 154 and Ho IX. DDO 154 is known to have a very large H I halo (Carignan & Beaulieu 1989; Carignan & Purton 1998). Because Ho IX is situated (in projection) very close to the spiral galaxy M 81, the H I for Ho IX is most likely a part of the overall gas distribution for M 81.

The bisector fit to the data (excluding DDO 165, Ho IX, and

¹¹ The proper interpretation of effective yields with respect to the “inner” and “outer” gas relative to the optical extent depends very strongly on the assumed metallicity of the outer gas, which is not known or well constrained in many nearby dwarf galaxies; however, see, e.g., Skillman et al. (1989); Kennicutt & Skillman (2001); Garnett (2002) for additional discussion. A detailed comparison between “non-scaled” and “scaled” H I content relative to the optical extent is outside the present focus of this paper.

NGC 1569) is shown as a solid line, and is expressed as

$$(B - [4.5]) = (2.79 \pm 0.11) + (-0.89 \pm 0.13) \log(M_{\text{gas}}/M_*), \quad (9)$$

and the dispersion in color is 0.32 mag. The fit also implies that $L_B/L_{[4.5]} \propto (M_{\text{gas}}/M_*)^{0.36}$. The strong correlation may simply reflect a more dominant process of the conversion of gas into stars. Galaxies with lower gas-to-stellar mass ratios have already depleted their fuel, and appear redder when present-day star formation no longer becomes active.

We consider possible departures from the closed-box model by inverting Equation (6) to obtain the effective yield, $y_{\text{eff}} = Z/\ln(\mu^{-1})$. The effective yield is determined simply from the measured oxygen abundances and baryonic gas fractions, and is equal to the true yield when the closed-box assumption applies. Effective yields which are smaller than the true yield suggest either outflow or infall of metal-poor gas (e.g., Edmunds 1990; Dalcanton 2006; van Zee & Haynes 2006). We have listed derived values of the effective yield in Table 5.

In Fig. 11a, we plot the effective yield as a function of the total baryonic mass, following Fig. 8 in Tremonti et al. (2004); Garnett (2002) also obtained a similar plot for a sample of nearby spiral and irregular galaxies. The empirical fit obtained by (Tremonti et al. 2004) is based upon the premise that galactic winds were responsible for metals loss; see also Veilleux et al. 2005 for additional discussion. From the present sample, there are dwarf galaxies with effective yields about a factor of ten lower than the “asymptotic” yield ($\log y_{\text{eff}} \approx -1.98$) for more massive galaxies in the SDSS. We have also marked for comparison the solar oxygen mass fraction ($\log Z_{\text{O},\odot} = -2.27$, Asplund et al. 2004; Meléndez 2004) and the effective yield for the nearby spiral M51 ($\log y_{\text{eff}} = -2.49$, Bresolin et al. 2004)¹². Accounting for the $\sim 0.2-0.3$ dex offset described above in § 4 lowers the “asymptotic” yield in better agreement with the solar mass fraction and the effective yield for M51. We note that these values are also comparable to the range of effective yields for dwarf galaxies (e.g., $\log y_{\text{eff}} \approx -2.7$ to -2.1) previously reported by, e.g., H. Lee et al. 2003b; van Zee & Haynes 2006).

Although there may be a trend between yield and baryonic mass for the low-mass galaxies, there is however large scatter, which is about 1.5 dex at $\sim 10^{8.5} M_{\odot}$. Three galaxies with the largest effective yields ($\log y_{\text{eff}} \gtrsim -2$) in our sample are DDO 154, NGC 3109, and Sextans A. However, their measured luminosities and abundances are in good agreement with other galaxies at comparable abundances and luminosities, respectively.

van Zee & Haynes (2006) observed a trend between effective yield and H I-gas-to- B -light ratio for a sample of nearby UGC dwarf galaxies, where the H I-gas-to- B -light ratio was a measure of the gas-to-stellar mass ratio. These authors ruled out infall of metal-poor gas as a mechanism to decrease effective yields (see also Dalcanton 2006). In Fig. 11b, we plot the effective yield as a function of the gas-to-stellar mass ratio. Gas-rich systems eventually reach the “asymptotic” yield, while gas-poor systems have lower effective yields. The effective yield is correlated with the gas-to-stellar mass ratio, and the fit is expressed as

$$\log y_{\text{eff}} = (-2.75 \pm 0.06) + (0.700 \pm 0.057) \log(M_{\text{gas}}/M_*) \quad (10)$$

¹² For a sample of H II regions in M51, Bresolin et al. (2004) measured electron temperatures from [N II] $\lambda 5755$ measurements, and derived chemical abundances. The subsequent effective yield for M51 was found to be lower by a factor of four than previous estimates.

with dispersion in log yield equal to 0.22 dex. In the limit of high gas fraction, the closed-box model predicts that the slope in equation above is equal to one.

6. RELATIONS WITH ROTATION VELOCITY

For a sample of dwarf irregular and spiral galaxies, Garnett (2002) found a relationship between metallicity and rotation velocity with an apparent “break” in the relation at 120 km s^{-1} . Pilyugin et al. (2004) performed a homogeneous analysis using his bright-line calibration, and found a similar break at 80 km s^{-1} . We plot various quantities against HI rotational velocity in Fig. 12, where the range of velocities for the present sample is between 10 and 80 km s^{-1} ; see Table 1. As an alternative to velocity on a linear scale, we plot the *logarithm* of the velocity.

In Fig. 12a, there appears to be a good correlation between stellar mass and rotation velocity ($r = +0.66$), although there is a paucity of data at low rotation velocity. The bisector fit is

$$\log M_* = (4.14 \pm 0.57) + (2.33 \pm 0.36) \log v_{\text{rot}}, \quad (11)$$

and the dispersion in log stellar mass is 0.63 dex. The fit can be inverted to give $v_{\text{rot}} \propto M_*^{0.43}$; the numerical exponent here is larger than the predicted value of 0.2 (Dekel & Woo 2003) by 3.4σ . The observational result suggests either larger rotation velocities at a given stellar mass, or smaller stellar masses at a given velocity.

In panels (b) and (c), respectively, we have plotted the gas-to-stellar mass ratio and the effective yield against rotation velocity. Neither panel reveals a strong trend, although the effective yield appears to rise slightly with rotation velocity. The rise of the effective yield with rotation velocity has been discussed by Garnett (2002), Pilyugin et al. (2004), and Dalcanton (2006). Galaxies with $v_{\text{rot}} \gtrsim 100 \text{ km s}^{-1}$ have effective yields approaching that of the asymptotic yield. Less massive galaxies with $v_{\text{rot}} \lesssim 100 \text{ km s}^{-1}$ have smaller effective yields which are roughly consistent with a solar-type yield, as seen above in Fig. 11. The present work suggests that the effective yield may be roughly constant, or at the very least, is weakly dependent upon rotation velocity. While additional data are required for confirmation, this result suggests that within the mass range of dwarf galaxies, the effective yield depends more strongly upon the relative gas fraction than upon rotation velocity.

7. DISCUSSION

We have shown that the scatter in the optical L - Z relation is constant (~ 0.16 dex) over a range of 11 mag in B luminosity, and the scatter decreases to 0.12 dex over 8 mag at NIR wavelengths. Our subsequent stellar mass-metallicity relation extends the dynamic range of the SDSS M_* - Z relation to lower masses by roughly 2.5 dex. We have also shown that the scatter for the M_* - Z relation appears to be similar over 5.5 orders of magnitude in stellar mass.

Models of galaxy formation have been successful in predicting the slopes of the L - Z and M_* - Z relations. These models generally incorporate feedback, which describes how effectively massive stars can inject energy into the surrounding interstellar medium. Dekel & Silk (1986) predicted the scaling relation, $L \propto Z^{2.7}$, for dwarf galaxies formed and embedded within dark matter haloes, although their model is less applicable to dwarf galaxies which have undergone a low and constant level of star formation over a Hubble time. The derived slopes of the L - Z relations (our Equation 2) are in

approximate agreement with the Dekel & Silk (1986) prediction, although our [4.5] L - Z slope is smaller than the predicted value by about 2σ . Recently, Dekel & Woo (2003) predicted the scaling relation $Z \propto M_*^{0.4}$. The slope of the M_* - Z relation in Equation (5) is smaller than the predicted value by 3.4σ . We note, however, that the Dekel & Woo (2003) scaling relation was derived for stellar iron metallicities under the assumption of constant [Fe/O], which may not be applicable in dwarf irregular galaxies (e.g., Smith et al. 2002).

Somerville & Primack (1999) compared predicted L - Z relations among a number of semi-analytical models. Although the details varied with the specific feedback recipe within the models, the scatter in the L - Z relations increased with decreasing total luminosity (their Fig. 18). Unfortunately, none of the models provided acceptable fits to all of the known observational parameters, and these authors stated that the failure of the models is likely caused by a strong difference in efficiency between ejecting gas and ejecting metals.

Models by De Lucia et al. (2004) produced M_* - Z relations consistent with the SDSS M_* - Z relation over a similar range in stellar mass, down to $\log(M_*/M_\odot) \sim 8.5$. Robertson et al. (2005) developed models to describe chemical abundance patterns observed in the Galactic halo, Local Group dwarf spheroidals, and Local Group dwarf irregular galaxies. They incorporated chemical enrichment histories and various gas accretion histories within cosmologically motivated Λ CDM models for the formation of dwarf galaxies and the Galactic stellar halo. Their models were able to reproduce the Dekel & Woo (2003) scaling relation and the observed abundance patterns in nearby dwarf galaxies.

Tremonti et al. (2004) explained that the relationship between stellar mass and metallicity was a consequence of the relationship between effective yield and total baryonic mass. That is, higher-mass systems are able to convert gas into stars which produce galaxies with large stellar masses and metallicities; whereas, lower-mass systems convert less gas into stars, and lose their metals as outflows by virtue of the lower total masses. These authors state: “... It is our view that the strong positive correlation between effective yield and baryonic mass is most naturally explained by the increasing potential barrier that the metal-laden wind must overcome to achieve ‘blowout.’ ...” In fact, since a number of the low-mass galaxies in our sample do not depart significantly from the L - Z and M_* - Z relationships and have effective yields close to or exceeding the asymptotic value, it is difficult to explain these relationships as a result of very disruptive blowout events.

Present-day galactic winds removing material from low-mass galaxies should have dramatic effects on the properties of such systems. We consider a prototype dwarf starburst galaxy, NGC 1569, which is undergoing blowout. Martin et al. (2002) showed in their *Chandra* observations that most of the oxygen produced in the starburst is in the enriched outflow. However, the results from (Martin et al. 2002, their Table 6) and Angeretti et al. (2005) reveal that at most 2% of the stellar mass is produced in the burst. Although the stellar mass ($\approx 10^{8.5} M_\odot$) of NGC 1569 is at the upper end of the range for our sample of dwarf galaxies, an equivalent NGC 1569-like burst would produce a more significant amount of stars in lower-mass systems. However, this high level of star formation is not presently seen in the other low-mass galaxies from our nearby sample, and certainly not seen in dwarf irregulars within the Local Group (cf. Mateo 1998).

We hypothesize that a less energetic form of metal-enhanced mass loss than blowouts could explain the small scatter in the $L-Z$ and M_*-Z relationships. Perhaps the slow loss of metals from an x-ray corona which is fed by individual supernova is sufficient to explain the observed relationships. Since this mechanism is an average over many events instead of depending on a small number of very energetic events, a smaller scatter would arise naturally. A low efficiency of star formation in dwarf irregular galaxies could account for a gentler form of mass loss.

While a number of the more massive dwarf galaxies in the present sample have experienced or will experience an outflow event (e.g., Summers et al. 2003; Hartwell et al. 2004; Grimes et al. 2005; Ott et al. 2005), the challenge remains to explain the uniform scatter in both the NIR $L-Z$ relation over a range of about 11 magnitudes in luminosity, and the M_*-Z relation over a range of about 5.5 decades in stellar mass. We suggest the following lines of research for the near future. New generations of models for galaxy formation which incorporate varying degrees of galaxy outflows should be able to predict the slope and the scatter in the $L-Z$ and M_*-Z relations. Large uniform surveys of galaxies are required to examine the percentage of stars formed in starbursts as a function of galaxy mass (e.g., Pérez-González et al. 2003). Results derived from the resolved stars in NGC 1569 (e.g., Angeretti et al. 2005) are promising, because similar studies will allow us to determine how much stellar mass has formed in the most recent bursts to a lookback time of a few Gyr. Additional NIR imaging and spectroscopy for a large number of dwarf galaxies within the Local Volume (Karachentsev et al. 2004) can test whether the scatter in the $L-Z$ and M_*-Z relations is truly comparable to the scatter in the respective relations for massive galaxies. With growing interest in understanding further the stages of galaxy assembly through $L-Z$ and M_*-Z diagnostics, improved models are crucial in providing further insights into the evolution of local and distant galaxies.

8. CONCLUSIONS

With *Spitzer* IRAC imaging, we have derived total near-infrared luminosities for 27 nearby dwarf irregular galaxies at 4.5 μm . The near-infrared $L-Z$ relation is constructed using 25 of these galaxies with secure distance and oxygen abundance measurements. While the slope of the subsequent [4.5] $L-Z$ relation is slightly smaller than the corresponding opti-

cal relations, the dispersion in the near-infrared $L-Z$ relation is reduced compared to the optical $L-Z$ relation. This result agrees with the expectation that variations in stellar mass-to-light ratios decrease from optical to near-infrared wavelengths. We constructed a M_*-Z relation, where the stellar masses were derived using color-based stellar mass-to-light ratios and corrected for the Chabrier IMF. The M_*-Z relation for dwarf galaxies extends the SDSS M_*-Z relation by another 2.5 decades. We find that the dispersion in the M_*-Z relation is comparable over 5.5 decades in stellar mass. The dispersions in the $L-Z$ and M_*-Z relations as well as the large variation in effective yields are difficult to understand if galactic superwinds or outflows are responsible for low metallicities at low mass or luminosity.

We thank the anonymous referee for their comments. This work is based in part on observations made with the *Spitzer Space Telescope*, which is operated by the Jet Propulsion Laboratory, California Institute of Technology under NASA contract 1407. Support for this work was provided by NASA through contracts 1256406 and 1215746 issued to the University of Minnesota by JPL/Caltech. H. L. is grateful to Eric Bell, Dominik Bomans, Andrew Cole, Chad Engelbracht, Ken Freeman, Karl Gordon, Valentin Ivanov, Rob Kennicutt, Chip Kobulnicky, Janice Lee, Marshall McCall, John Moustakas, Michael Richer, Jessica Rosenberg, H el ene Rousel, John Salzer, Ivo Saviane, Rachel Somerville, Christy Tremonti, and Liese van Zee for their comments, suggestions, and words of wisdom. H. L. also thanks Julianne Dalcanton, Claudia Mendes de Oliveira, and Sonia Temporin for copies of their manuscripts before publication. H. L. and E. D. S. acknowledge partial support from a NASA LTSARP grant NAG 5-9221 and the University of Minnesota. This research was partially supported by a grant from the American Astronomical Society. Some data were accessed as Guest User, Canadian Astronomy Data Center, which is operated by the Dominion Astrophysical Observatory for the National Research Council of Canada's Herzberg Institute of Astrophysics. This research has made use of NASA's Astrophysics Data System, and of the NASA/IPAC Extragalactic Database (NED), which is operated by the Jet Propulsion Laboratory, California Institute of Technology, under contract with the National Aeronautics and Space Administration.

REFERENCES

- Akritas, M. G., & Bershad, M. A. 1996, *ApJ*, 470, 706
Allamandola, L. J., Tielens, A. G. G. M., & Barker, J. R. 1985, *ApJ*, 290, L25
Angeretti, L., Tosi, M., Greggio, L., Sabbi, E., Aloisi, A., & Leitherer, C. 2005, *AJ*, 129, 2203
Aparicio, A. 1994, *ApJ*, 437, L27
Asplund, M., Grevesse, N., Sauval, A. J., Allende Prieto, C., & Kiselman, D. 2004, *A&A*, 417, 751
Bell, E. F., & Bower, R. G. 2000, *MNRAS*, 319, 235
Bell, E. F., & de Jong, R. S. 2001, *ApJ*, 550, 212
Bell, E. F., McIntosh, D. H., Katz, N., & Weinberg, M. D. 2003, *ApJS*, 149, 289
Bessell, M. S., & Brett, J. M. 1988, *PASP*, 100, 1134
B oker, T., van der Marel, R. P., Mazza, L., Rix, H.-W., Rudnick, G., Ho, L. C., & Shields, J. C. 2001, *AJ*, 121, 1473
Bresolin, F., Garnett, D. R., & Kennicutt, R. C. 2004, *ApJ*, 615, 228
Campins, H., Rieke, G. H., & Lebofsky, M. J. 1985, *AJ*, 90, 896
Carigi, L., Col n, P., & Peimbert, M. 2006, *ApJ*, submitted (astro-ph/0509829)
Carignan, C., & Beaulieu, S. 1989, *ApJ*, 347, 760
Carignan, C., & Purton, C. 1998, *ApJ*, 506, 125
Chabrier, G. 2003, *PASP*, 115, 763
Clementini, G., Held, E. V., Baldacci, L., & Rizzi, L. 2003, *ApJ*, 588, L85
Cole, A. A., et al. 1999, *AJ*, 118, 1657
Dalcanton, J. 2006, *ApJ*, submitted
Dale, D. A., et al. 2005, *ApJ*, 633, 857
De Lucia, G., Kauffmann, G., & White, S. D. M. 2004, *MNRAS*, 349, 1101
Dekel, A., & Silk, J. 1986, *ApJ*, 303, 39
Dekel, A., & Woo, J. 2003, *MNRAS*, 344, 1131
Devost, D., Roy, J.-R., & Drissen, L. 1997, *ApJ*, 482, 765
Dohm-Palmer, R. C., et al. 1998, *AJ*, 116, 1227
Dolphin, A. E. 2000, *ApJ*, 531, 804
Dolphin, A. E., et al. 2001, *ApJ*, 550, 554
Dolphin, A. E., et al. 2003, *AJ*, 125, 1261
Drozdovsky, I. O., Schulte-Ladbeck, R. E., Hopp, U., Greggio, L., & Crone, M. M. 2002, *ApJ*, 124, 811
Edmunds, M. G. 1990, *MNRAS*, 246, 678
Engelbracht, C. W., Gordon, K. D., Rieke, G. H., Werner, M. W., Dale, D. A., & Latter, W. B. 2005, *ApJ*, 628, L29
Erb, D. K., Shapley, A. E., Pettini, M., Steidel, C. C., Reddy, N. A., & Adelberger, K. L. 2006, *ApJ*, in press (astro-ph/0602473)
Fazio, G. G., et al. 2004, *ApJS*, 154, 10
Ferrarese, L., et al. 2000, *ApJS*, 128, 431
Frei, Z., & Gunn, J. E. 1994, *AJ*, 108, 1476
Gallart, C., Aparicio, A., Bertelli, G., & Chiosi, C. 1996, *AJ*, 112, 1928
Gallazzi, A., Charlot, S., Brinchmann, J., White, S. D. M., & Tremonti, C. A. 2005, *MNRAS*, 362, 41

- Galliano, F. 2005, in "The Spectral Energy Distributions of Gas-Rich Galaxies: Confronting Models with Data", eds. C. C. Popescu, & R. J. Tuffs, AIP Conf. Proc. 761, 231
- Garnett, D. R. 2002, *ApJ*, 581, 1019
- González-Delgado, R. M. et al. 1994, *ApJ*, 437, 239
- Grimes, J. P., Heckman, T., Strickland, D., & Ptak, A. 2005, *ApJ*, 628, 187
- Hartwell, J. M., Stevens, I. R., Strickland, D. K., Heckman, T. M., & Summers, L. K. 2004, *MNRAS*, 348, 406
- Hidalgo-Gómez, A. M., Sánchez-Salcedo, F. J., & Olofsson, K. 2003, *A&A*, 399, 63
- Hogg, D. W., Tremonti, C. A., Blanton, M. R., Finkbeiner, D. P., Padmanabhan, N., Quintero, A. D., Schlegel, D. J., & Wherry, N. 2005, *ApJ*, 624, 162
- Hora, J. L. et al. 2004, in Proceedings of the SPIE Vol. 5487, "Microwave and Terahertz Photonics", ed. A. Stohr, D. Jager, & S. Iezekiel, 77
- Houck, D. W. et al. 2004, *ApJS*, 154, 211
- Hoyos, C., Koo, D. C., Phillips, A. C., Willmer, C. N. A., & Guhathakurta, P. 2005, *ApJ*, 635, L21
- Hunter, D. A., & Hoffman, L. 1999, *AJ*, 117, 2789
- Indebetouw, R. et al. 2005, *ApJ*, 619, 931
- Israel, F. P. 1988, *A&A*, 194, 24
- Izotov, Y. I., Thuan, T. X., & Lipovetsky, V. A. 1997, *ApJS*, 108, 1
- Jackson, D. C., Cannon, J. M., Skillman, E. D., Lee, H., Gehrz, R. D., Woodward, C. E., & Polomski, E. 2006, *ApJ*, in press (astro-ph/0603860)
- Jarrett, T. H., Chester, T., Cutri, R., Schneider, S. E., & Huchra, J. P. 2003, *AJ*, 125, 525
- Karachentsev, I. D., et al. 2002a, *A&A*, 383, 125
- Karachentsev, I. D., et al. 2002b, *A&A*, 385, 21
- Karachentsev, I. D., et al. 2002c, *A&A*, 389, 812
- Karachentsev, I. D., et al. 2003a, *A&A*, 398, 467
- Karachentsev, I. D., et al. 2003b, *A&A*, 404, 93
- Karachentsev, I. D., Karachentseva, V. E., Huchtmeier, W. K., & Makarov, D. I. 2004, *AJ*, 127, 2031
- Kennicutt, R. C., & Skillman, E. D. 2001, *AJ*, 121, 1461
- Kennicutt, R. C., Bresolin, F., & Garnett, D. R. 2003a, *ApJ*, 591, 801
- Kennicutt, R. C. et al. 2003b, *PASP*, 115, 928
- Kniazev, A. Y., Grebel, E. K., Pustilnik, S. A., Pramskij, A. G., & Zucker, D. B. 2005, *AJ*, 130, 1558
- Kobulnicky, H. A., & Kewley, L. J. 2004, *ApJ*, 617, 240
- Kobulnicky, H. A., & Skillman, E. D. 1996, *ApJ*, 471, 211
- Kobulnicky, H. A., & Skillman, E. D. 1997, *ApJ*, 489, 636
- Kobulnicky, H. A., & Zaritsky, D. 1999, *ApJ*, 511, 118
- Kobulnicky, H. A., Skillman, E. D., Roy, J., Walsh, J. R., & Rosa, M. R. 1997, *ApJ*, 477, 679
- Kobulnicky, H. A., Kennicutt, R. C. Jr., & Pizagno, J. L. 1999, *ApJ*, 514, 544
- Kobulnicky, H. A., et al. 2003, *ApJ*, 599, 1006
- Kroupa, P. 2001, *MNRAS*, 322, 231
- Lamareille, F., Contini, T., Brinchmann, J., Le Borgne, J.-F., Charlot, S., & Richard, J. 2006, *A&A*, 448, 907
- Lee, H., Grebel, E. K., & Hodge, P. W. 2003a, *A&A*, 401, 141
- Lee, H., McCall, M. L., Kingsburgh, R., Ross, R., & Stevenson, C. C. 2003b, *AJ*, 125, 146
- Lee, H., McCall, M. L., & Richer, M. G. 2003c, *AJ*, 125, 2975
- Lee, H., & Skillman, E. D. 2004, *ApJ*, 614, 698
- Lee, H., Skillman, E. D., & Venn, K. A. 2005, *ApJ*, 620, 223
- Lee, H., Skillman, E. D., & Venn, K. A. 2006a, *ApJ*, 642, 813
- Lee, H., Zucker, D. B., & Grebel, E. K. 2006b, *ApJ*, in preparation
- Lee, J. C., Salzer, J. J., & Melbourne, J. 2004, *ApJ*, 616, 752
- Léger, A., & Puget, J. L. 1984, *A&A*, 137, L5
- Lequeux, J., Peimbert, M., Rayo, J. F., Serrano, A., & Torres-Peimbert, S. 1979, *A&A*, 80, 155
- Liang, Y. C., Hammer, F., Flores, H., Elbaz, D., Marcellac, D., & Cesarsky, C. J. 2004, *A&A*, 423, 867
- Liang, Y. C., Hammer, F., & Flores, H. 2006, *A&A*, 447, 113
- Lu, N., Helou, G., Werner, M. W., Dinerstein, H. L., Dale, D. A., Silberman, N. A., Malhotra, S., Beichman, C. A., & Jarrett, T. H. 2003, *ApJ*, 588, 199
- Lu, N. 2004, *ApJS*, 154, 286
- Lutz, D. 1999, in "The Universe as Seen by ISO", eds. P. Cox & M. F. Kessler. ESA-SP 427, 623
- Lynds, R., Tolstoy, E., O'Neil Jr., E. J., & Hunter, D. A. 1998, *AJ*, 116, 146
- Magrini, L., Leisy, P., Corradi, R. L. M., Perinotto, M., Mampaso, M., & Vílchez, J. M. 2005, *A&A*, 443, 115
- Maier, C., Lilly, S. J., Carollo, M., Stockton, A., & Brodwin, M. 2005, *ApJ*, 634, 849
- Makarova, L., Karachentsev, I., Takalo, L. O., Heinämäki, P., & Valtonen, M. 1998, *A&AS*, 128, 459
- Martin, C. 1997, *ApJ*, 491, 561
- Martin, C., Kobulnicky, H. A., & Heckman, T. M. 2002, *ApJ*, 574, 663
- Masegosa, J., Moles, M., & del Olmo, A. 1991, *A&A*, 249, 505
- Masegosa, J., Moles, M., & Campos-Aguilar, A. 1994, *ApJ*, 420, 576
- Massey, P., Hodge, P. W., Holmes, S., Jacoby, G., King, N. L., Olsen, K., Smith, C., & Saha, A. 2002, *BAAS*, 34, 1272
- Mateo, M. 1998, *ARA&A*, 36, 435
- McGaugh, S. S. 1991, *ApJ*, 380, 140
- Meléndez, J. 2004, *ApJ*, 615, 1042
- Méndez, B., Davis, M., Moustakas, J., Newman, J., Madore, B. F., & Freedman, W. L. 2002, *AJ*, 124, 213
- Miller, B. W. 1995, *ApJ*, 446, L75
- Miller, B. W., & Hodge, P. W. 1996, *ApJ*, 458, 467
- Minniti, D., & Zijlstra, A. A. 1997, *AJ*, 114, 147
- Minniti, D., Zijlstra, A. A., & Alonso, M. V. 1999, *AJ*, 117, 881
- Moles, M., Aparicio, A., & Masegosa, J. 1990, *A&A*, 228, 310
- Musella, I., Píotto, G., & Capaccioli, M. 1997, *AJ*, 114, 976
- Oliveira, C. M., Temporin, S., Cypriano, E. S., Plana, H., Amram, P., Sodré Jr., L., & Balkowski, C. 2006, *AJ*, in press (astro-ph/0602288)
- Ott, J., Walter, F., & Brinks, E. 2005, *MNRAS*, 358, 1453
- Pahre, M. A., Ashby, M. L. N., Fazio, G. G., & Willner, S. P. 2004, *ApJS*, 154, 235
- Peimbert, A., Peimbert, M., & Ruiz, M. T. 2005, *ApJ*, 634, 1056
- Pérez-González, P. G., Gil de Paz, A., Zamorano, J., Gallego, J., Alonso-Herrero, A., & Aragón-Salamanca, A. 2003, *MNRAS*, 338, 525
- Pietrzyński, G., Gieren, W., Udalski, A., Bresolin, F., Kudritzki, R., Soszyński, I., Szymański, M., & Kubiak, M. 2004, *AJ*, 128, 2815
- Pilyugin, L. S. 2001, *A&A*, 374, 412
- Plyugin, L. S., Vílchez, J. M., & Contini, T. 2004, *A&A*, 425, 849
- Piotto, G., Capaccioli, M., & Pellegrini, C. 1994, *A&A*, 287, 371
- Pritchett, C. J., Schade, D., Richer, H. B., Crabtree, D., Yee, H. K. C. 1987, *ApJ*, 323, 79
- Reach, W. T. et al. 2005, *PASP*, 117, 978
- Rejkuba, M., Minniti, D., Gregg, M. D., Zijlstra, A. A., Victoria Alonso, M., & Goudfrooij, P. 2000, *AJ*, 120, 801
- Richer, M. G., & McCall, M. L. 1995, *ApJ*, 445, 642
- Robertson, B., Bullock, J. S., Font, A. S., Johnston, K. V., & Hernquist, L. 2005, *ApJ*, 632, 872
- Rosenberg, J. L., Ashby, M. L. N., Salzer, J. J., & Huang, J.-S. 2006, *ApJ*, 636, 742
- Roussel, H., Gil de Paz, A., Seibert, M., Helou, G., Madore, B. F., & Martin, C. 2005, *ApJ*, 632, 227
- Sakai, S., Madore, B. F., & Freedman, W. L. 1996, *ApJ*, 461, 713
- Sakai, S., Madore, B. F., & Freedman, W. L. 1997, *ApJ*, 480, 589
- Salpeter, E. E. 1955, *ApJ*, 121, 161
- Salzer, J. J., Lee, J. C., Melbourne, J., Hinz, J. L., Alonso-Herrero, A., & Jangren, A. 2005, *ApJ*, 624, 661
- Savaglio, S. et al. 2005, *ApJ*, 635, 260
- Saviane, I., Held, E. V., Ivanov, V., Alloin, D., Bresolin, F., Rich, R. M., Rizzi, L., & Momany, Y. 2005, in "Near-Field Cosmology with Dwarf Elliptical Galaxies", Proc. IAU Colloquium No. 198, ed. B. Binggeli & H. Jerjen (astro-ph/0505341)
- Schmidt, M. 1963, *ApJ*, 137, 758
- Schulte-Ladbeck, R. E., Crone, M. M., & Hopp, U. 1998, *ApJ*, 493, L23
- Searle, L., & Sargent, W. L. W. 1972, *ApJ*, 173, 25
- Shapley, A. E., Erb, D. K., Pettini, M., Steidel, C. C., & Adelberger, K. L. 2004, *ApJ*, 612, 108
- Shapley, A. E., Coil, A. L., Ma, C.-P., & Bundy, K. 2005, *ApJ*, 635, 1006
- Skillman, E. D., Bomans, D. J., & Kobulnicky, H. A. 1997, *ApJ*, 474, 205
- Skillman, E. D., Côté, S., & Miller, B. W. 2003, *AJ*, 125, 610
- Skillman, E. D., Kennicutt, R. C., Jr., & Hodge, P. W. 1989, *ApJ*, 347, 875
- Smith, V. V. et al. 2002, *AJ*, 124, 3241
- Smerville, R. S., & Primack, J. R. 1999, *MNRAS*, 310, 1087
- Stasińska, G. 2002, *Rev. Mexicana Astron. Astrofis. Ser. Conf.* 12, Ionized Gaseous Nebulae, ed. W. J. Henney et al. (Mexico D.F.: UNAM), 62
- Stasińska, G., Comte, G., & Vigroux, L. 1986, *A&A*, 154, 352
- Summers, L. K., Stevens, I. R., Strickland, D. K., & Heckman, T. M. 2003, *MNRAS*, 342, 690
- Talent, D. L. 1980, Ph.D. thesis, Rice University
- Tamura, N., Hirashita, H., & Takeuchi, T. T. 2001, *ApJ*, 552, L113
- Thuan, T. X., & Izotov, Y. I. 2005, *ApJ*, 627, 739
- Tikhonov, N. A., Galazutdinova, O. A., & Drozdovsky, I. O. 2005, *A&A*, 431, 127
- Tissera, P. B., De Rossi, M. E., & Scannapieco, C. 2005, *MNRAS*, 364, L38
- Tolstoy, E., Gallagher, J. S., Cole, A. A., Hoessel, J. G., Dohm-Palmer, R. C., Skillman, E. D., Mateo, M., & Hurley-Keller, D. 1998, *AJ*, 116, 1244
- Tosi, M., Sabbi, E., Bellazzini, M., Aloisi, A., Greggio, L., Leitherer, C., & Montegriffo, P. 2001, *AJ*, 122, 1271
- Tremonti, C. A., et al. 2004, *ApJ*, 613, 898
- Tüllmann, R., Rosa, M. R., Elwert, T., Bomans, D. J., Ferguson, A. M. N., & Dettmar, R.-J. 2003, *A&A*, 412, 69
- Tumlinson, J. 2006, *ApJ*, submitted (astro-ph/0602179)
- Webster, B. L., & Smith, M. G. 1983, *MNRAS*, 204, 743
- Vaduvescu, O., McCall, M. L., Richer, M. G., & Fingerhut, R. L. 2005, *AJ*, 130, 1593
- van den Bosch, F. C. 2002, *MNRAS*, 332, 456
- van Zee, L., & Haynes, M. 2006, *ApJ*, 636, 214
- van Zee, L., Haynes, M. P., & Salzer, J. J. 1997, *AJ*, 114, 2479
- van Zee, L., Skillman, E. D., & Haynes, M. 2006, *ApJ*, 637, 269
- Veilleux, S., Cecil, G., & Bland-Hawthorn, J. 2005, *ARA&A*, 43, 769
- Waller, W. H. 1991, *ApJ*, 370, 144
- Werner, M. W., et al. 2004, *ApJS*, 154, 1
- Zaritsky, D., Kennicutt, R. C., & Huchra, J. P. 1994, *ApJ*, 420, 87

TABLE 1
 PROPERTIES FOR 27 NEARBY ($D \lesssim 5$ MPC) DWARF IRREGULAR GALAXIES.

Galaxy	Source	AORKEY (G128)	$F_{[4.5]}$ (mJy)	$m-M$ (mag)	Distance Refs.	$M_{[4.5]}$ (mag)	Nebular 12+log(O/H) (dex)	O/H Refs.	$B-[4.5]$ (mag)	log M_* (M_\odot)
(1)	(2)	(3)	(4)	(5)	(6)	(7)	(8)	(9)	(10)	(11)
DDO 154	S	...	2.42 ± 0.24	27.53 ± 0.10	1	-15.28 ± 0.10	7.67 ± 0.05	1,2	1.88	6.68
DDO 165	S	...	9.57 ± 0.96	28.30 ± 0.19	2	-17.62 ± 0.19	2.46	7.73
DDO 53	S	...	2.97 ± 0.30	27.76 ± 0.15	2	-15.73 ± 0.15	7.62 ± 0.20	3	2.36	6.98
GR 8 ^a	G128	5054464	2.95 ± 0.30	26.75 ± 0.35	3	-14.72 ± 0.35	7.64 ± 0.04	4	2.52	6.62
Ho I	S	...	4.40 ± 0.44	27.92 ± 0.26	1	-16.32 ± 0.26	7.70 ± 0.20	5	1.83	7.08
Ho II	S	...	42.9 ± 4.3	27.65 ± 0.13	1	-18.53 ± 0.13	7.93 ± 0.05	6,7	1.82	7.96
Ho IX	S	...	2.72 ± 0.27	27.80 ± 0.08^b	...	-15.75 ± 0.10	... ^b	...	2.07	6.89
IC 1613	G128	5051648	91.53 ± 9.2	24.22 ± 0.10	4,5	-15.92 ± 0.10	7.62 ± 0.05	8	1.42	6.82
IC 2574	S	...	70.1 ± 7.0	28.02 ± 0.22	1	-19.43 ± 0.22	8.15 ± 0.11	5,6	2.09	8.39
IC 5152	G128	5055232	149 ± 15	26.58 ± 0.18	6	-18.28 ± 0.18	7.92 ± 0.07	8	2.78	8.11
Leo A	G128	5052416	8.65 ± 0.87	24.2 ± 0.2	7	-13.34 ± 0.20	7.35 ± 0.06	4	1.84	5.89
M81 dwB ^a	S	...	2.72 ± 0.27	28.62 ± 0.10	1	-16.50 ± 0.10	7.98 ± 0.22	5	1.96	7.19
NGC 1569	G69	...	220 ± 22	26.71 ± 0.60	8	-19.36 ± 0.60	8.19 ± 0.02	9–11	0.93	8.07
NGC 1705	S	...	17.4 ± 1.7	28.54 ± 0.26	9	-18.44 ± 0.26	8.21 ± 0.05	12	2.62	8.13
NGC 2366	G69	...	35.2 ± 3.5	27.52 ± 0.28	1,10	-18.18 ± 0.28	7.91 ± 0.08	13,14	2.18	7.91
NGC 3109	G128	5052928	131 ± 13	25.52 ± 0.18	11–13	-17.61 ± 0.10	8.06 ± 0.20	7,15,16	1.11	7.41
NGC 3738	G69	...	32.8 ± 3.3	28.45 ± 0.25	14	-19.03 ± 0.25	8.23 ± 0.01	11	2.45	8.32
NGC 4214	G69	...	175 ± 18	27.13 ± 0.20	15	-19.53 ± 0.20	8.22 ± 0.05	17	2.55	8.55
NGC 4449	G69	...	303 ± 30	28.12 ± 0.27	14	-21.12 ± 0.27	8.31 ± 0.07	11,18	2.98	9.29
NGC 5408	S	...	27.2 ± 2.7	28.41 ± 0.17	16	-18.79 ± 0.17	7.98 ± 0.01	19,20	2.29	8.19
NGC 55	G128	5056000	785 ± 79	25.85 ± 0.20	17–19	-19.88 ± 0.20	8.05 ± 0.10	21–23	1.58	8.44
NGC 6822	S	...	1440 ± 140	23.49 ± 0.08	20–22	-18.14 ± 0.10	8.11 ± 0.10	24,25	2.98	8.10
Peg DIG ^a	G128	5055744	30.5 ± 3.1	24.90 ± 0.10	23	-15.40 ± 0.10	7.93 ± 0.13	26	2.90	6.98
Sextans A	G128	5053696	8.39 ± 0.84	25.75 ± 0.15	24–26	-14.85 ± 0.15	7.54 ± 0.06	1,27,28	0.85	6.24
Sextans B	G128	5052672	23.0 ± 2.3	25.63 ± 0.04	6,13,24,27	-15.83 ± 0.10	7.53 ± 0.05	15,27–29	1.73	6.86
UGC 6456	G59	...	2.25 ± 0.23	28.19 ± 0.04	13,28,29	-15.87 ± 0.10	7.69 ± 0.07	11,14,30,31	1.83	6.90
WLM	G128	5051136	45.8 ± 4.6	24.83 ± 0.08	31–33	-15.78 ± 0.10	7.83 ± 0.06	32	1.88	6.88

NOTE. — Col. (1): Galaxy name (alphabetical order). Col. (2): Data source: G59 — GTO 59 (P.I. G. Rieke), G69 — GTO 69 (P.I. G. Fazio), G128 — GTO 128 (P.I. R. D. Gehrz), and S — SINGS (159; Kennicutt et al. 2003b). Col. (3): AOR Key pertaining to galaxies observed in program GTO 128. Col. (4): Flux density at $4.5 \mu\text{m}$. Our measured flux densities for SINGS galaxies are consistent with those found in Dale et al. (2005); see also Fig. 3. Cols. (5) and (6): Distance modulus and references, respectively. Col. (7): Absolute magnitude at $4.5 \mu\text{m}$. Cols. (8) and (9): Nebular (H II region) oxygen abundance and references, respectively. Col. (10): Derived $B-[4.5]$ colors in the present work, where B magnitudes are corrected for Galactic extinctions; see Karachentsev et al. (2004). Col. (11): Derived stellar mass using model 8 in Table 3, and adjusted downwards by 0.25 dex for the Chabrier (2003) IMF.

REFERENCES. — Distance references: 1. Makarova et al. 1998; 2. Karachentsev et al. 2002a; 3. Dohm-Palmer et al. 1998; 4. Cole et al. 1999; 5. Dolphin et al. 2001; 6. Karachentsev et al. 2002c; 7. Tolstoy et al. 1998; 8. Angeretti et al. 2005; 9. Tosi et al. 2001; 10. Thuan & Izotov 2005; 11. Musella et al. 1997; 12. Minniti et al. 1999; 13. Méndez et al. 2002; 14. Karachentsev et al. 2003a; 15. Drozdovsky et al. 2002; 16. Karachentsev et al. 2002b; 17. Pritchett et al. 1987; 18. Karachentsev et al. 2003b; 19. Tikhonov et al. 2005; 20. Gallart et al. 1996; 21. Clementini et al. 2003; 22. Pietrzyński et al. 2004; 23. Aparicio 1994; 24. Piotto et al. 1994; 25. Sakai et al. 1996; 26. Dolphin et al. 2003; 27. Sakai et al. 1997; 28. Lynds et al. 1998; 29. Schulte-Ladbeck et al. 1998; 30. Minniti & Zijlstra 1997; 31. Dolphin 2000; 32. Rejkuba et al. 2000.

Spectroscopic oxygen abundance references: 1. van Zee et al. 1997; 2. Kennicutt & Skillman 2001; 3. Skillman et al. 1989; 4. van Zee et al. 2006; 5. Miller & Hodge 1996; 6. Masegosa et al. 1991; 7. H. Lee et al. 2003b; 8. H. Lee et al. 2003a; 9. Devost et al. 1997; 10. Kobulnicky & Skillman 1997; 11. Martin 1997; 12. H. Lee & Skillman 2004; 13. González-Delgado et al. 1994; 14. Izotov et al. 1997; 15. H. Lee et al. 2006b; 16. Richer & McCall 1995; 17. Kobulnicky & Skillman 1996; 18. Böker et al. 2001; 19. Stasińska et al. 1986; 20. Masegosa et al. 1994; 21. Talent 1980; 22. Webster & Smith 1983; 23. Tüllmann et al. 2003; 24. Peimbert et al. 2005; 25. H. Lee et al. 2006a; 26. Skillman et al. 1997; 27. Kniazev et al. 2005; 28. Magrini et al. 2005; 29. Moles et al. 1990; 30. Lynds et al. 1998; 31. Hunter & Hoffman 1999; 32. H. Lee et al. 2005.

^aAlternative names: GR 8 — DDO 155, UGC 8091; M81 dwB — UGC 5423; Pegasus dwarf irregular (Peg DIG) — DDO 216, UGC 12613.

^bHo IX: We have adopted the distance to M 81 (Ferrarese et al. 2000). Miller (1995) measured $12+\log(\text{O}/\text{H}) \sim 8.0 \pm 0.2$ from a supernova remnant.

TABLE 2
COMPARISON AMONG SELECTED LUMINOSITY-METALLICITY RELATIONS FOR NEARBY DWARF IRREGULAR GALAXIES AND OTHER DISTANT STAR-FORMING GALAXIES. WE SHOW HERE A NUMBER OF $L-Z$ RELATIONS FROM THE LITERATURE; THIS IS NOT INTENDED TO BE A COMPLETE LISTING. WE HAVE NOT PERFORMED A HOMOGENEOUS TREATMENT OF THE DATA LISTED IN THIS TABLE.

Data source (1)	No. of Galaxies (2)	Luminosity Range (3)	Wavelength (μm) (4)	$L-Z$ fits		a_{16} (7)	Dispersion in $\log(\text{O}/\text{H})$ (dex) (8)
				a (5)	b (6)		
Local galaxies ($D \lesssim 10$ Mpc)							
This paper	25	$-11 \gtrsim M_B \gtrsim -18$	4.5	5.78 ± 0.21	-0.122 ± 0.012	7.73	0.12
This paper	25	$-11 \gtrsim M_B \gtrsim -18$	0.4 (B)	5.94 ± 0.27	-0.128 ± 0.017	7.99	0.16
Oliveira et al. 2006	29	$-12 \gtrsim M_B \gtrsim -18$	2.2 (K_s)	5.55 ± 0.26	-0.14 ± 0.02	7.79	0.15
van Zee et al. 2006	33	$-11 \gtrsim M_B \gtrsim -18$	0.4 (B)	5.65 ± 0.17	-0.149 ± 0.011	8.03	0.15
H. Lee et al. 2003b	22	$-11 \gtrsim M_B \gtrsim -18$	0.4 (B)	5.59 ± 0.54	-0.153 ± 0.025	8.04	0.18
Richer & McCall 1995	21	$-11 \gtrsim M_B \gtrsim -18$	0.4 (B)	5.67 ± 0.48	-0.147 ± 0.029	8.02	0.08 ^a
Skillman et al. 1989	20	$-11 \gtrsim M_B \gtrsim -19$	0.4 (B)	5.50	-0.153	7.95	0.16
Distant galaxies							
Rosenberg et al. 2006	17	$-16 \gtrsim M_B \gtrsim -18$	3.6	4.85	-0.16	7.41	0.16
Salzer et al. 2005	370	$-12 \gtrsim M_B \gtrsim -22$	2.2 (K)	3.92 ± 0.09	-0.212 ± 0.003	7.31	0.24
Savaglio et al. 2005	79	$-18 \gtrsim M_B \gtrsim -22$	0.4 (B)	2.98 ± 0.94	-0.280 ± 0.045	7.46	...
Kobulnicky & Kewley 2004	177	$-17 \gtrsim M_B \gtrsim -22$	0.4 (B)	4.90	-0.193	7.99	...
J. Lee et al. 2004	54	$-12 \gtrsim M_B \gtrsim -20$	0.4 (B)	5.37 ± 0.46	-0.159 ± 0.029	7.91	0.26
Tremonti et al. 2004	$\gtrsim 53000$	$-16 \gtrsim M_B \gtrsim -22$	0.4 (B) ^b	5.238 ± 0.018	-0.185 ± 0.001	8.20	0.16

NOTE. — Col. (1): Reference. Col. (2): Number of galaxies. Col. (3): Luminosity range. A number of the studies quote B, AB magnitudes, which are 0.163 mag brighter than Johnson B magnitudes (Frei & Gunn 1994). Col. (4): Wavelength. Cols. (5) and (6): Fits to the respective relations are expressed as $12+\log(\text{O}/\text{H}) = a + bM_\lambda$, where a and b are the intercept and the slope, respectively, and M_λ is the absolute magnitude at wavelength λ . Col. (7): a_{16} represents the oxygen abundance determined from the specified relation at a fiducial galaxy luminosity equal to $M_\lambda = -16$. Col. (8): Dispersion in oxygen abundance.

^a Richer & McCall (1995) stated the fit parameters and resulting dispersion were effective only for galaxies brighter than $M_B = -15$, as the dispersion increased towards lower luminosities. However, H. Lee et al. (2003b) showed that improved data (e.g., distances) reduced the dispersion at lower luminosities.

^b Tremonti et al. (2004) obtained galaxy luminosities in Sloan filter g (similar to B), and accounted for the appropriate transformations from g to B .

TABLE 3

STELLAR MASSES USING MODELS OF STELLAR MASS-TO-LIGHT RATIOS FROM TABLES 3 AND 4 IN BELL & DE JONG (2001) AND THE METHOD DESCRIBED IN § 4. FROM THE RESULTING DERIVED STELLAR MASSES, WE PERFORMED THE RESULTING M_* - Z FIT FOR EACH MODEL. WE LIST EACH M_* - Z FIT AS $12+\log(\text{O}/\text{H}) = a + b \log M_*$, AND WE LIST THE DISPERSION IN OXYGEN ABUNDANCE FOR EACH FIT.

Model # (1)	Model (2)	$B-V$		$V-K$		$B-K$		M_* - Z fits		Dispersion in $\log(\text{O}/\text{H})$ (dex) (11)
		a_K (3)	b_K (4)	a_K (5)	b_K (6)	a' (7)	b' (8)	a (9)	b (10)	
Scaled Salpeter IMF, Z_\odot										
1	Closed box	-0.554	0.540	-0.740	0.207	-0.688	0.150	5.52 ± 0.24	0.307 ± 0.031	0.118
2	Infall	-0.692	0.699	-0.926	0.258	-0.863	0.188	5.57 ± 0.23	0.304 ± 0.030	0.117
3	Outflow	-0.534	0.500	-0.622	0.157	-0.601	0.119	5.49 ± 0.24	0.309 ± 0.031	0.118
4	Dynamical time	-0.531	0.476	-0.687	0.177	-0.645	0.129	5.50 ± 0.23	0.309 ± 0.030	0.118
5	Formation epoch	-0.694	0.676	-0.966	0.270	-0.888	0.193	5.58 ± 0.23	0.303 ± 0.030	0.117
6	Form. epoch: bursts	-0.692	0.652	-1.087	0.314	-0.959	0.212	5.60 ± 0.23	0.302 ± 0.030	0.117
7	Cole et al. (2000)	-0.654	0.696	-1.019	0.301	-0.909	0.210	5.58 ± 0.23	0.302 ± 0.030	0.117
Different SPS ^a Models (IMFs); $0.4 Z_\odot$										
8	BC Salpeter	-0.43	0.60	-1.16	0.44	-0.851	0.254	5.58 ± 0.23	0.298 ± 0.030	0.117
9	BC scaled Salpeter	-0.59	0.60	-1.31	0.44	-1.005	0.254	5.62 ± 0.23	0.298 ± 0.030	0.117
10	BC modif. Salpeter	-0.71	0.60	-1.45	0.45	-1.133	0.257	5.66 ± 0.22	0.297 ± 0.029	0.117
11	BC96 Scalo	-0.65	0.56	-1.36	0.43	-1.052	0.243	5.64 ± 0.23	0.299 ± 0.030	0.117
12	KA Salpeter	-0.38	0.53	-1.03	0.39	-0.754	0.225	5.55 ± 0.24	0.300 ± 0.030	0.117
13	Schulz et al. Salpeter	-0.65	0.77	-2.50	0.81	-1.552	0.395	5.81 ± 0.22	0.284 ± 0.030	0.120
14	Pégase Salpeter	-0.38	0.59	-1.15	0.45	-0.817	0.255	5.57 ± 0.24	0.298 ± 0.030	0.117
15	Pégase $x = -1.85$	-0.07	0.48	-0.71	0.37	-0.431	0.209	5.45 ± 0.24	0.301 ± 0.030	0.117
16	Pégase $x = -0.85$	-0.59	0.71	-1.25	0.45	-0.994	0.275	5.62 ± 0.23	0.296 ± 0.030	0.117

NOTE. — Col. (1): Model number. Col. (2): Model type. BC – Bruzual & Charlot, KA – Kodama & Arimoto; see Bell & de Jong (2001) for details. Cols. (3) and (4): Intercept and slope, respectively, for $\log(M_*/L_K)$ as a linear function of $B-V$. Cols. (5) and (6): Intercept and slope, respectively, for $\log(M_*/L_K)$ as a linear function of $V-K$. Cols. (7) and (8): Derived intercept and slope, respectively, for $\log(M_*/L_K)$ as a linear function of $B-K$. Cols. (9) and (10): Derived intercept and slope, respectively, for the subsequent M_* - Z fits for the given model. Cols. (11): Dispersion in $\log(\text{O}/\text{H})$.

^a SPS models - stellar population synthesis models.

TABLE 4

COMPARISON AMONG SELECTED STELLAR MASS-METALLICITY RELATIONS FOR NEARBY DWARF IRREGULAR GALAXIES AND STAR-FORMING GALAXIES AT DISTANT EPOCHS. FITS TO THE RESPECTIVE RELATIONS ARE EXPRESSED AS $12+\log(\text{O}/\text{H}) = f(X)$, OR FUNCTIONS OF $X = \log M_*$. WE HAVE NOT HOMOGENIZED MEASURES OF THE STELLAR MASS OR METALLICITY FOR THE OTHER STUDIES. THIS IS NOT A COMPLETE LISTING, AS WE HAVE SELECTED RECENTLY PUBLISHED M_* - Z RELATIONS FROM THE LITERATURE.

Data source	No. of Galaxies	Redshift	Luminosity Range	M_* - Z fits ($X = \log M_*$)	Dispersion in $\log(\text{O}/\text{H})$ (dex)
This paper	25	$\lesssim 0.001$	$-13 \gtrsim M_{[4.5]} \gtrsim -21$	$(5.54 \pm 0.24) + (0.298 \pm 0.030)X$	0.12
Savaglio et al. 2005	56	~ 0.7	$-18 \gtrsim M_{B,AB} \gtrsim -22$	$(4.06 \pm 0.58) + (0.478 \pm 0.058)X$	0.20
Tremonti et al. 2004	$\gtrsim 53000$	~ 0.1	$-16 \gtrsim M_B \gtrsim -22$	$-1.492 + 1.847X - 0.080X^2$	0.10
Pérez-González et al. 2003	163	~ 0.026	$-19 \gtrsim M_K \gtrsim -26$	$(6.02 \pm 0.28) + (0.257 \pm 0.028)X$	0.21

TABLE 5
GAS-TO-STELLAR MASS FRACTIONS AND EFFECTIVE YIELDS.

Galaxy (1)	F_{21} (Jy km s ⁻¹) (2)	$\log(M_{\text{gas}}/M_*)$ (3)	$\log y_{\text{eff}}$ (4)	v_{rot} (km s ⁻¹) (5)
DDO 154	145	2.00	-1.26	54
DDO 165	28.2	0.55	...	23
DDO 53	13.8	0.770	-2.51	17
GR 8	8.6	0.464	-2.75	21
Ho I	38.9	1.18	-2.03	18
Ho II	363	1.17	-1.82	56
Ho IX	158	1.93	...	50
IC 1613	698	1.26	-2.04	19
IC 2574	447	0.97	-1.90	55
IC 5152	98.0	0.02	-2.84	50
Leo A	68.4	1.13	-2.49	4
M81 dwB	3.8	0.34	-2.52	25
NGC 1569	74.1	-0.01	-2.59	37
NGC 1705	16.6	0.02	-2.55	61
NGC 2366	295	1.07	-1.93	45
NGC 3109	1110	1.39	-1.47	51
NGC 3738	21.9	-0.09	-2.61	50
NGC 4214	324	0.32	-2.30	43
NGC 4449	794	0.36	-2.18	84
NGC 5408	64.6	0.49	-2.37	33
NGC 55	2679	1.15	-1.72	78
NGC 6822	2399	0.17	-2.54	55
Peg DIG	22.8	-0.36	-3.07	8
Sextans A	208.8	1.83	-1.56	49
Sextans B	102.4	0.92	-2.45	22
UGC 6456	14.1	1.03	-2.19	7
WLM	299.8	1.03	-2.05	26

NOTE. — Col. (1): Galaxy name. Col. (2): 21-cm flux densities (Karachentsev et al. 2004). Col. (3): Gas-to-stellar mass ratio. Col. (4): Logarithm of the effective yield. Col. (5): H I rotational velocity corrected for inclination and turbulent motions (Karachentsev et al. 2004).

FIG. 1.— Postage-stamp images at $4.5 \mu\text{m}$ of dwarf galaxies from GTO 128. North and East are at the top and left, respectively, in each frame. All galaxies are displayed with the same isophotal scaling to emphasize the large range in surface brightness of the dwarf galaxies. The fields of view shown are: GR 8 — $5' \times 5'$, IC 1613 — $10' \times 10'$, IC 5152 — $5' \times 5'$, Leo A — $5' \times 5'$, NGC 55 — $15' \times 10'$, NGC 3109 — $10' \times 5'$, Peg DIG — $5' \times 5'$, Sextans A — $5' \times 5'$, Sextans B — $5' \times 5'$, and WLM — $5' \times 15'$.

FIG. 2.— Example of galaxy photometry for Sextans B. North and East are to the top and left, respectively, in the $4.5 \mu\text{m}$ image. The central elliptical aperture surrounds the galaxy, and the seven circular apertures sample the background flux. The galaxy aperture is aligned roughly to the same orientation as the optical emission seen on images from the Digitized Sky Survey.

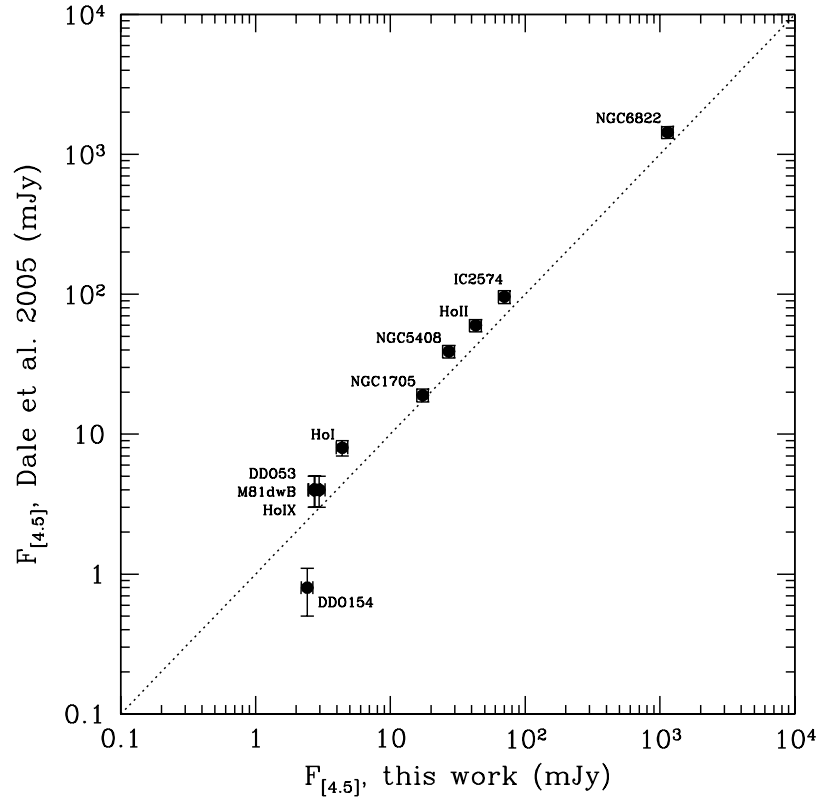


FIG. 3.— Comparison of total $4.5 \mu\text{m}$ fluxes for selected dwarf galaxies from the SINGS sample: fluxes from Dale et al. (2005) versus measured fluxes from the present work. The dotted line marks the line of equal fluxes.

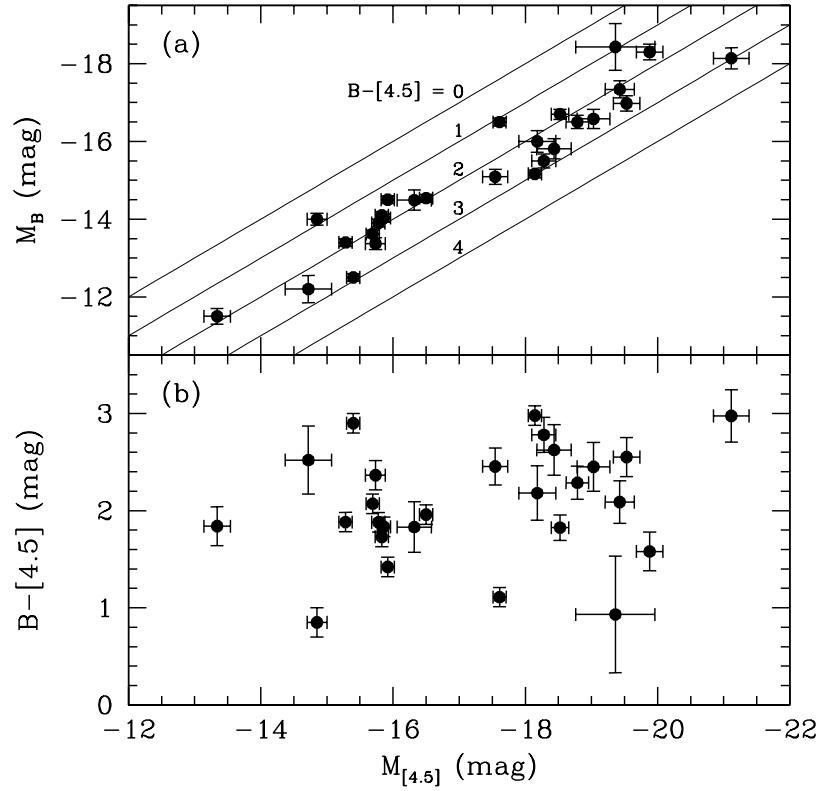


FIG. 4.— (a) B absolute magnitude versus $[4.5]$ absolute magnitude. Lines of constant $B-[4.5]$ color between 0 and 4 are also plotted. (b) $B-[4.5]$ color versus $[4.5]$ absolute magnitude. The Pearson correlation coefficient for this color-magnitude relation is $r = -0.24$.

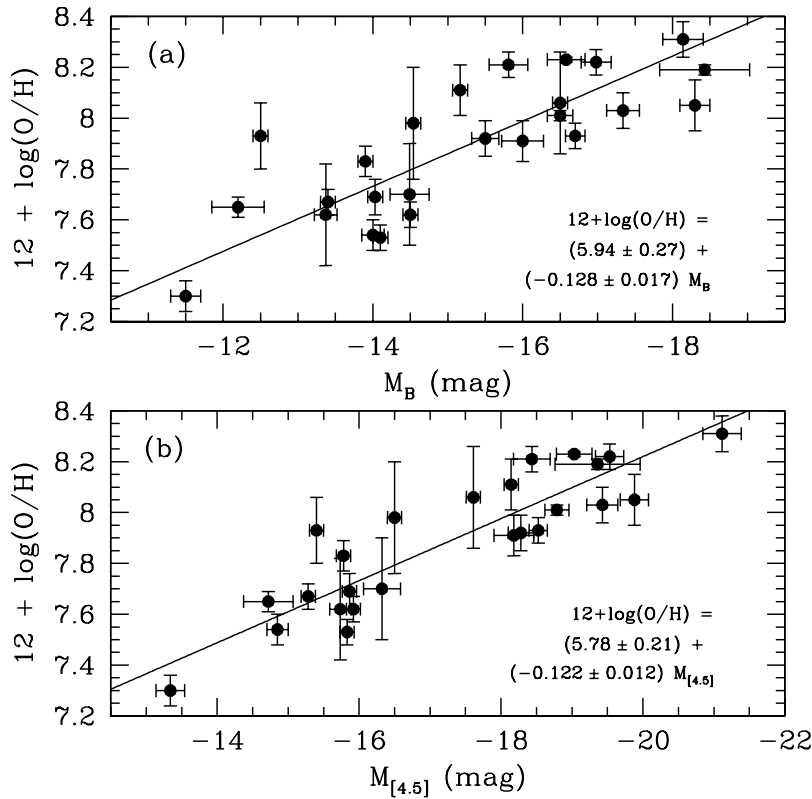


FIG. 5.— Nebular oxygen abundances versus (a) absolute magnitude in B , and (b) absolute magnitude at $4.5 \mu\text{m}$. The solid lines represent fits to the data, whose fit parameters are given in each panel. The Pearson coefficients are $r = -0.80$ in B , and $r = -0.89$ in $[4.5]$.

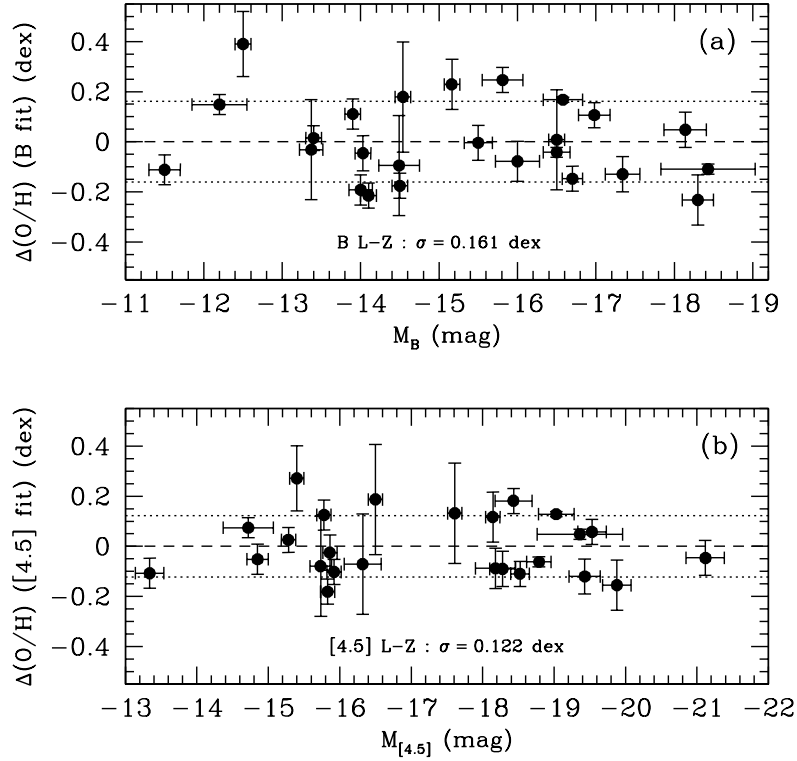


FIG. 6.— (a) Residuals in oxygen abundance (from B fit) versus B absolute magnitude. (b) Residuals in oxygen abundance (from [4.5] fit) versus [4.5] absolute magnitude. Both panels are plotted to the same vertical scale, and a short-dashed horizontal line in each panel indicates zero residual. The dotted horizontal lines in each panel indicate the 1σ scatter. The scatter in the NIR $L-Z$ relation is reduced compared to that found in the $B\ L-Z$ relation.

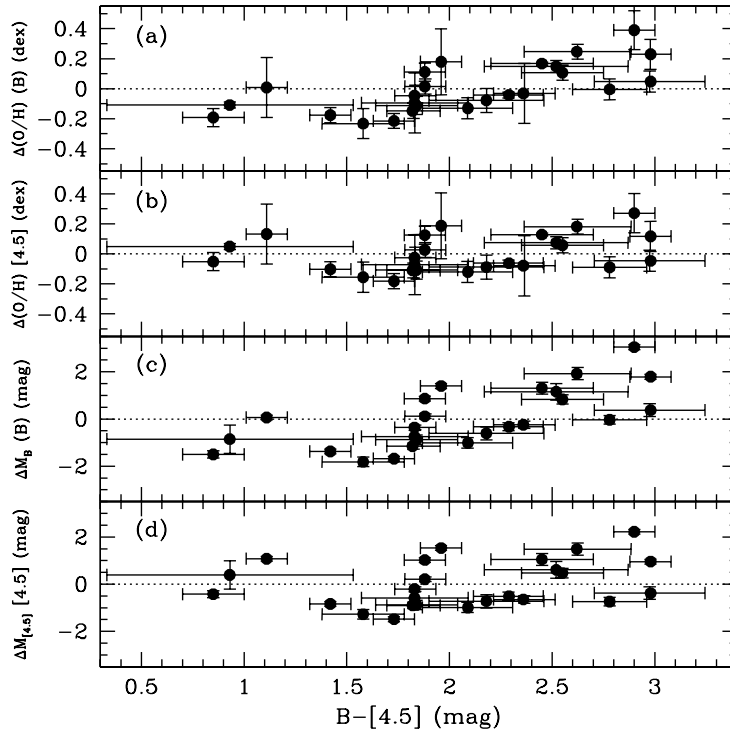


FIG. 7.— Panel (a): Residuals in oxygen abundance from the $B\ L-Z$ fit versus $B-[4.5]$ color. Panel (b): Residuals in oxygen abundance from the [4.5] $L-Z$ fit versus $B-[4.5]$ color. Panels (a) and (b) are plotted to the same vertical scale. Panel (c): Residuals in B absolute magnitude from the $B\ L-Z$ fit versus $B-[4.5]$ color. Panel (d): Residuals in [4.5] absolute magnitude from the [4.5] $L-Z$ fit versus $B-[4.5]$ color. Panels (c) and (d) are plotted to the same vertical scale. Residuals at optical wavelengths correlate ($r = +0.67$) more strongly with $B-[4.5]$ color than residuals at NIR wavelengths ($r = +0.28$).

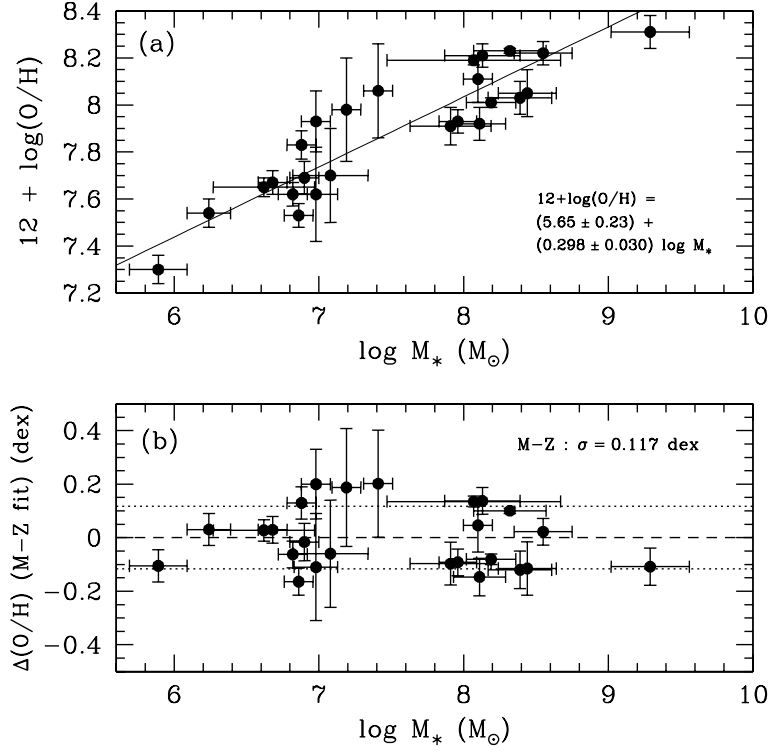


FIG. 8.— Panel (a): oxygen abundance versus stellar mass. Stellar masses have been derived using the color-based stellar mass-to-light ratios from model 8 in Table 3, and have been corrected to the Chabrier (2003) IMF. The fit to the data is shown as the solid line; the Pearson coefficient is $r = +0.90$. Panel (b): residuals in oxygen abundance from our present M_* - Z relation against stellar mass. The Pearson coefficient is $r = -0.08$.

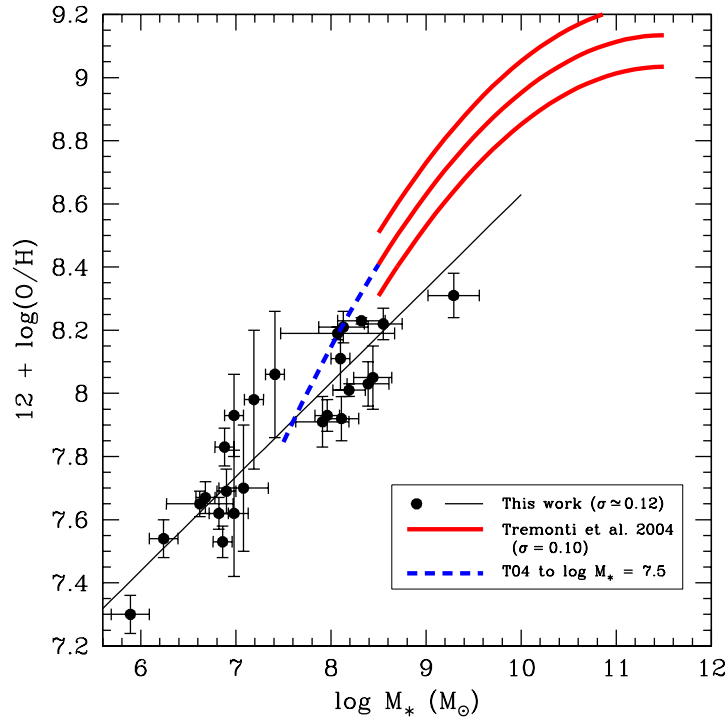


FIG. 9.— Oxygen abundance versus stellar mass. The plot has been expanded to include more massive galaxies. Data and the least-squares fit to the present data from Fig. 8 are shown; the fit is shown as a thin black solid line and is arbitrarily extrapolated to $10^{10} M_\odot$. The polynomial fit to over 53000 galaxies from the SDSS (Tremonti et al. 2004) is shown as a heavy red solid line; the 1σ curves are also shown. Their fit is effective over the mass range between $8.5 \lesssim \log(M_*/M_\odot) \lesssim 11.5$. In the “overlap region” ($8.5 \lesssim \log(M_*/M_\odot) \lesssim 9.5$), SDSS galaxies are more metal-rich by ≈ 0.2 – 0.3 dex compared to dwarf galaxies in the present sample. An extrapolation of the SDSS M_* - Z relation down to $\log(M_*/M_\odot) = 7.5$ is shown as a blue short-dashed line.

FIG. 10.— Panels (a) and (b): oxygen abundances are plotted against gas-to-stellar mass ratio. In panel (a), the solid line represents the fit to the data; the Pearson coefficient is $r = -0.58$. In panel (b), we have plotted outflow variations of the closed-box model, where the outflow rate is a constant multiple of the star-formation rate. The purple and blue curves describe models with $y_O = 0.01$ (Tremonti et al. 2004) and $y_O = 2 \times 10^{-3}$ (e.g., H. Lee et al. 2003b; van Zee & Haynes 2006), respectively. For each set of curves, the outflow rates from right to left are 0, 5, 10, 25, and 50 times the star-formation rate, respectively. In panel (c), $B-[4.5]$ colors are plotted against gas-to-stellar mass ratio. The solid line represents the fit, and the Pearson coefficient is $r = -0.83$. The fit excludes DDO 165, Ho IX, and NGC 1569; the latter is the outlier with a very blue color for its relatively low gas-to-stellar mass ratio.

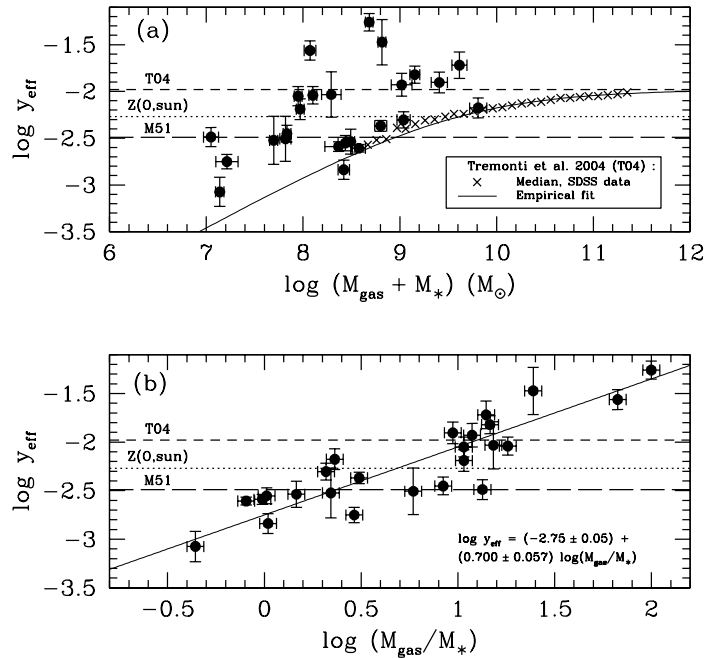


FIG. 11.— Panel (a): effective yield against total baryonic mass in gas and stars; cf. also Garnett (2002). Filled circles represent dwarf galaxies in the present work. Crosses represent the median of the SDSS data in mass bins of 0.1 dex (Tremonti et al. 2004). The empirical fit is shown as a thin solid line (Tremonti et al. 2004, their Equation 6). The asymptotic yield ($y_{\text{eff}} = 0.0104$) is represented by the short-dashed line. The solar oxygen mass fraction (Asplund et al. 2004; Meléndez 2004) and the effective yield for the nearby spiral galaxy M51 (Bresolin et al. 2004) are represented by dotted and long-dashed lines, respectively. These values are comparable to the range of effective yields for dwarf galaxies (e.g., $\log y_{\text{eff}} \simeq -2.7$ to -2.1 , H. Lee et al. 2003b; van Zee & Haynes 2006). Panel (b): effective yield versus gas-to-stellar mass ratio. The fit shown is represented by a thin solid line. The trend here is similar to the one observed for a sample of nearby UGC dwarf galaxies described by van Zee & Haynes (2006). The horizontal lines are the same as in the panel above.

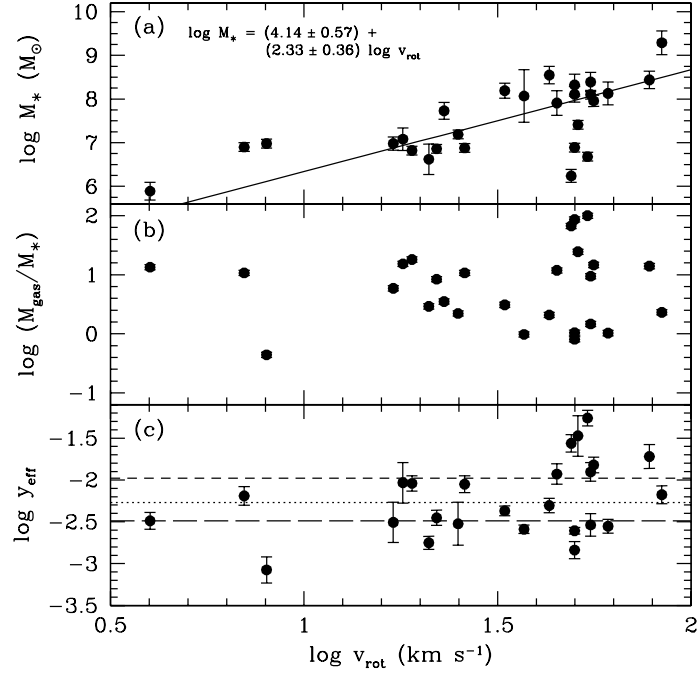


FIG. 12.— Panel (a): stellar mass versus H I rotation velocity. The solid line represents the fit to the data with Pearson coefficient $r = +0.67$. Panel (b): gas-to-stellar mass ratio versus H I rotation velocity. Panel (c): effective yield versus H I rotation velocity. H I rotation velocities in Table 1 have been corrected for inclination and turbulent motions; see Karachentsev et al. (2004). The Pearson correlation coefficient between rotation velocity and effective yield is $r = +0.40$. The horizontal lines are the same as in Fig. 11.

This figure "f1.jpg" is available in "jpg" format from:

<http://arxiv.org/ps/astro-ph/0605036v1>

This figure "f2.jpg" is available in "jpg" format from:

<http://arxiv.org/ps/astro-ph/0605036v1>

This figure "f10.jpg" is available in "jpg" format from:

<http://arxiv.org/ps/astro-ph/0605036v1>